Diplomarbeit

Base Metal Nitrosyl Pincer Complexes

ausgeführt zum Zwecke der Erlangung des akademischen Grades eines

Diplom-Ingenieurs

unter der Leitung von

Prof. DI Dr. Karl Kirchner

eingereicht an der Technischen Universität Wien
Fakultät für Technische Chemie
von

Jan Pecak

Wien, Penzing

Wien, im Jänner 2018 _____

Jan Pecak

Ich habe zur Kenntnis genommen, dass ich zur Drucklegung meiner Arbeit unter der Bezeichnung

Diplomarbeit

nur mit Bewilligung der Prüfungskommission berechtigt bin.

Ich erkläre weiters Eides statt, dass ich meine Diplomarbeit nach den anerkannten Grundsätzen für wissenschaftliche Abhandlungen selbstständig ausgeführt habe und alle verwendeten Hilfsmittel, insbesondere die zugrunde gelegte Literatur, genannt habe.

Weiters erkläre ich, dass ich dieses Diplomarbeitsthema bisher weder im In- noch Ausland (einer Beurteilerin/einem Beurteiler zur Begutachtung) in irgendeiner Form als Prüfungsarbeit vorgelegt habe und dass diese Arbeit mit der vom Begutachter beurteilten Arbeit übereinstimmt.

Wien, im Jänner 2018

_____

Jan   Pecak

Acknowledgment

First of all, I would like to express my sincere gratitude to Prof. Karl Kirchner for giving me the opportunity to work on my master thesis in his research group and for supervising me during this time.

I would also like to acknowledge Berthold Stöger, not only for introducing me into XRD and for valuable comments on this thesis, but also for innumerable eventful evenings.

Furthermore I would like to mention my friends and colleagues Viktor Wessely, Alexander Viernstein, Klaus Dobrezberger and Clara Schweinzer as well as Julian Brünig, Wolfgang Eder, Mathias Glatz, Nikolaus Gorgas, Daniel Himmelbauer, Esther Knittl, Matthias Mastalir, Markus Rotter, Gerald Tomsu and Stefan Weber from the inorganic chemistry department. Thank you for your support and numerous amusing hours!

Moreover, I would like to express my special thanks to Sarah for her love, mental support and wonderful time spent together.

Finally, I would like express my deepest gratitude to my parents for providing me with unfailing support throughout the years. This accomplishment would not have been possible without them.

Kurzfassung

Ein bedeutendes Betätigungsfeld der modernen anorganischen Chemie behandelt die Synthese und Charakterisierung von Übergangsmetallkomplexen mit Pincer Liganden. Das besondere Interesse an diesen Systemen gründet auf der großen Variabilität und Flexibilität bei der Synthese dieser Liganden und der Möglichkeit das Metallzentrum auf diese Weise elektronisch und sterisch zu beeinflussen. Obgleich es mittlerweile eine Vielzahl von Arbeiten zur Synthese und Anwendung solcher Komplexe gibt, behandeln nur sehr wenige die Einführung des Stickstoffmonoxid Liganden in diese Chemie. Stickstoffmonoxid (NO) ist der bekannteste Vertreter der sog. nicht unschuldigen Liganden welche in der Lage sind, in verschieden Arten an ein Metall zu binden und während einer Reaktion den Bindungsmodus zu wechseln.

Im Zuge dieser Arbeit wurden neue Wege zur Darstellung von NO Komplexen unedler Metalle (Mn, Fe, Co) untersucht. Eine Reihe von bislang unbekannten low spin Eisen PNP Nitrosyl Komplexen der Art $[Fe(PNP)(NO)X]^+$ (X = Cl, Br) wurde durch Reaktion von $[Fe(PNP)X_2]$ mit Nitrosonium Salzen (z.B. $NOBF_4$) oder Stickstoffmonoxid in Lösung dargestellt. Weiteres wurde die Reaktivität der gleichen Fe(II) Komplexe gegenüber NO im Festkörper untersucht und mit dem bekannten chemischen Verhalten von Kohlenmonoxid verglichen. Die isolierten Produkte wurden mittels Röntgenbeugung, IR-, Mössbauer- und EPR-Spektroskopie charakterisiert und ihre elektronische Struktur mittels DFT untersucht.

Abstract

The investigation of pincer ligands and their transition metal complexes has received significant attention in the last years. Due to easily achievable modifications in their molecular scaffold, they provide for a huge variability and a rich chemistry. Although there a numerous works dealing with the preparation of pincer complexes bearing ligands such as halides, carbon monoxide, hydrides or borohydrides, there are only few reports in conjunction with nitric oxide. NO is the most prominent example of a redox non-innocent ligand able to bind to a metal center in various bonding modes, i.e. the linear and the bent mode and to interconvert during chemical transformations.

In the course of this thesis new pathways to prepare base metal (i.e., Mn, Fe, Co) pincer nitrosyl complexes were investigated. A series of low spin iron PNP nitrosyl complexes of the kind $[Fe(PNP)(NO)X]^+$ (X = Cl, Br) was prepared by reacting $[Fe(PNP)X_2]$ with nitrosonium salts (e.g. $NOBF_4$) or NO in solution. Moreover, the reactivity of the same precursor complexes towards NO in solid state was investigated and compared to the known chemical behavior towards CO. The isolated compounds were characterized by means of X-Ray diffraction, IR-, Mössbauer and EPR-Spectroscopy and studied by means of DFT.

Table of content

1 Introduction

An important area of research in modern inorganic and organometallic chemistry comprises the development of new transition metal compounds. In this context the investigation of pincer complexes and their diverse chemistry attracted significant attention over the last years particularly with regard to their applicability in homogeneous catalysis.[1,2] When considering the behavior of ligands coordinated to metal centers, two classifications arise: Ancillary ligands (e.g. pincer ligands) are defined as supporting ligands that can modulate the reactivity of the metal center while reactive ligands (e.g. CO, H) undergo chemical transformations or dissociate from the metal. The introduction of nitric oxide (NO), as a reactive or ancillary ligand into pincer chemistry therefore bears potential regarding reactivity and the possibility of new reaction paths in catalytic applications. NO is the most prominent example of a redox non-innocent ligand able to bind to a metal center in various bonding modes, i.e. the linear and the bent mode and to interconvert during chemical transformations via electron transfer between the metal center and the ligand. The linear nitrosyl can be viewed as an NO^+ group which is isoelectronic to carbon monoxide, CO. Although there is a formal similarity between those two ligands there are only few nitrosyl pincer complexes reported in literature and their behavior is poorly investigated. On the other hand here is plethora of known (and stable) transition metal complexes (based both on noble and base metals) that incorporate carbon monoxide as a ligand. Especially the chemistry of iron PNP pincer complexes has been profoundly investigated in the last years and numerous preparative routes have been established.

This work deals with the promising conjunction of already established iron pincer chemistry with NO as a ligand, a comparison of the CO and NO ligand systems regarding their reactivity and stability and new preparative approaches towards iron nitrosyl pincer complexes.

1.1 Pincer ligands

Pincer ligands[3,4] constitute a class of tridentate chelating ligands based on an aromatic or aliphatic framework. Attached to this framework via linkers (X) are donating groups (E) such as phosphines, amines or carbenes. Bonding to a metal center can then occur via donating groups E and E' and Y on the organic scaffold (Fig. 1). These structurally rather rigid ligand systems usually impose a meridional coordination mode and a planar geometry when forming a metal complex. Since their first appearance in literature[5] in the 1970ies, the chemistry of pincer ligands and their complexes developed to an important field of research in organometallic and coordination chemistry. The advantage of pincer ligands lies in the high stability of their transition metal complexes, in the imposition of unusual reaction pathways and their behavior as cooperating ligands. Due to possible and often easily achievable structural variation in the framework and attached donating groups, pincer ligands provide for a huge variability and reactivity.
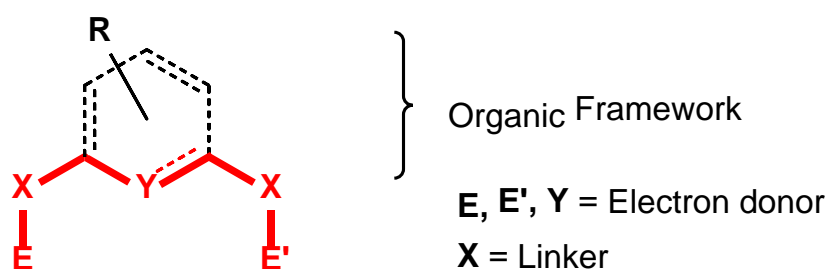
R

X—Y—X

E   E'

Organic Framework

E, E', Y = Electron donor

X = Linker

Fig. 1 General constitution of a tridentate pincer type ligand

1.2 Structural variety of pincer ligands

The structural variety of pincer ligands and their related electronic properties is based upon the fact that a great number of known aromatic (i.e. heterocyclic) and aliphatic chemical systems can be transformed into such ligands. Therefore, numerous pincer ligands were developed over the last two decades and applied as supporting ligands for virtually all metals throughout the periodic system of elements. Fig. 2 shows an overview of published and applied pincer ligands based on aliphatic and aromatic scaffolds. Donating groups (E, E' and Y) within these ligands are usually systems based on the elements N, C, P and S. Linking groups (X) include NR', CH_2 and O. Moreover various organic substituents (R) can be attached to the scaffold in order to

modulate electronic and steric properties or to enable immobilization on solid supports for catalytic applications.

Moreover, both the scaffold and the donor groups can be used to introduce chirality into the ligand or complex in order to achieve stereo selective reactivity.
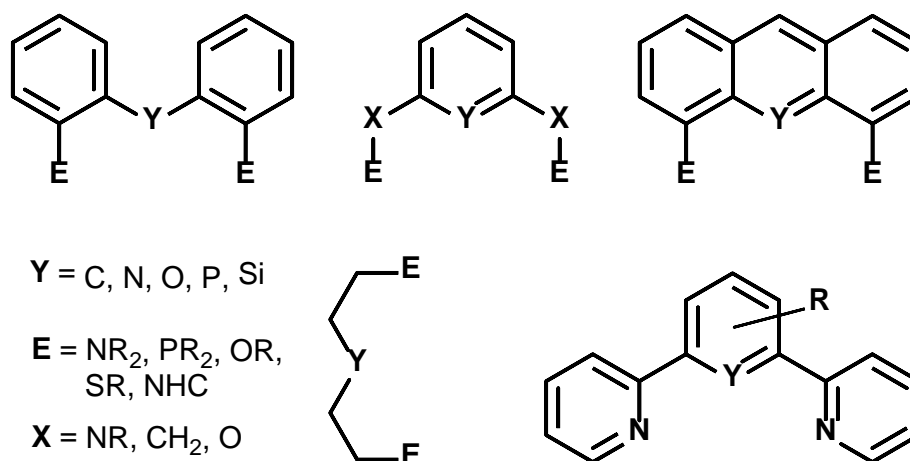

Y = C, N, O, P, Si

E = NR$_2$, PR$_2$, OR, SR, NHC

X = NR, CH$_2$, O

Fig. 2 Overview of aliphatic and aromatic pincer ligands

1.3   PNP Ligands

A synthetically simple yet powerful approach to preparing pincer ligands is based on the use of 2,6-diaminopyridine (Y = N) and related heterocyclic systems. In conjunction with phosphine groups (E = P) very useful ligands can be obtained. Fig. 3 shows the general structure of a PNP ligand with an N-heterocyclic (pyridine, pyrimidine and triazine) scaffold, potential linking groups (X = CH$_2$, NR and O) and phosphines or phosphites PR$_2$ (R = Me, *i*Pr, Ph, *t*Bu, OMe, ETOL) as donors. By varying the linking atoms and the substituents in PR$_2$ controlling and tuning of the ligands properties is easily achievable. Furthermore, chirality can be introduced by preparing chiral phosphines or phosphites such as BINOL or TADDOL.
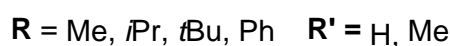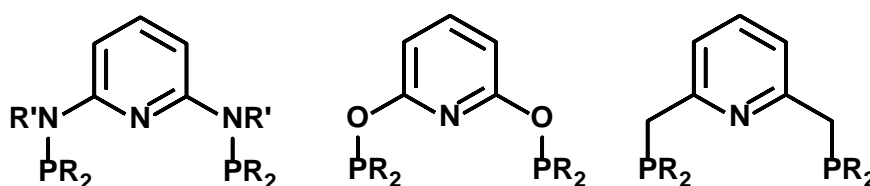

R = Me, *i*Pr, *t*Bu, Ph   **R' =** H, Me

Fig. 3 Pyridine based PNP ligands with different linking groups

The synthetic approach towards simple PNP ligands is usually based on a one-step synthesis (Fig. 4) by reacting a 2,6-diamino[6] or 2,6-dihydroxy[7] substituted aromatic system (such as pyridine) with a chlorophosphine Cl-PR$_2$ in the presence of a weak base. For the preparation of CH$_2$ linked[8] PNP ligands 2,6-dimethylpyrdine (lutidine) can be treated with nBuLi (for deprotonation) and chlorophosphine, subsequently.
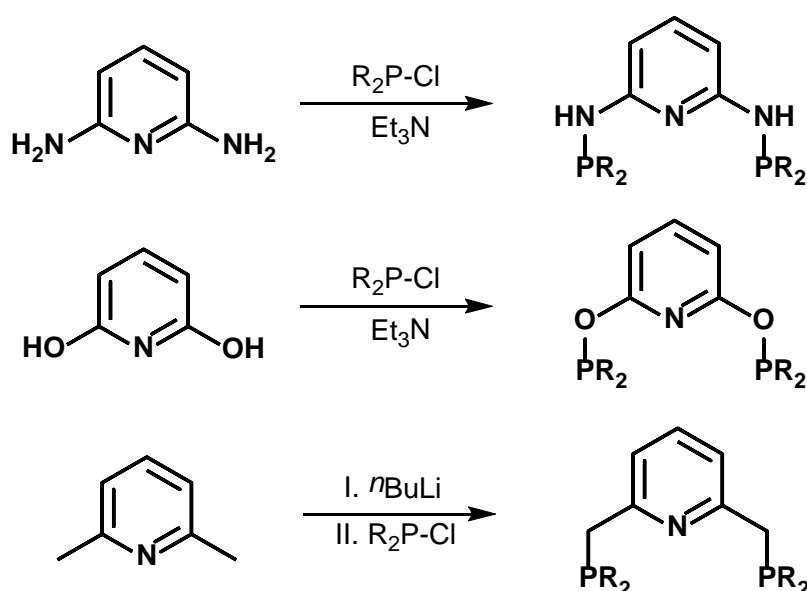

Fig. 4 Synthetic approaches towards NH, O and CH$_2$ linked PNP ligands
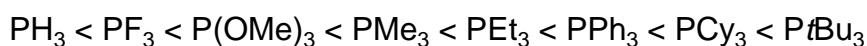
1.4   Phosphines

The coordination ability and donor strength of a PNP pincer ligand is primarily based on the phosphorous groups involved. Phosphines, PR$_3$, constitute a series of ancillary ligands in which electronic and steric properties can be altered in a systematic way. In analogy to an amine, phosphines have an electron lone pair on the phosphorous atom that can be donated to a metal (two electron donor) and form an σ-bond. In contrast to NH$_3$, phosphines possess capabilities for backbonding owing to their π-acidity. This electronic effect can be altered and controlled by

variation of the substituents R on PR_3 and thereby altering the energy of the σ^* orbitals of the P-R bonds, which plays the role of the acceptor in PR_3. Whenever the R group becomes more electronegative, the σ^* orbital becomes more stable and its energy is lowered. As a consequence, lowering the orbital energy of the empty antibonding orbital increases accessibility for back donation and the π-acidity as described in the series below:

$$PMe_3 \approx P(NR_2)_3 < PAr_3 < P(OMe)_3 < P(OAr)_3 < PCl_3 < CO \approx PF_3$$

The electronic effect of various phosphines was quantified by Tolman[9] in 1977 by comparing the $\nu(CO)$ wave numbers of a series of Nickel complexes containing different PR_3 ligands. The stronger donor phosphines (left side) increase the electron density in the metal center, which passes some this charge to the CO ligands by backdonation. This effect in turn leads to a decrease in $\nu(CO)$ of the particular complex. The second parameter introduced by Tolman is the cone angle θ which describes the steric attributes of phosphines. In the same way as above the steric demand can be adjusted by variation of R groups as shown in the series below. In this way electronic effects can be changed without significantly changing the steric size or vice versa.

$$PH_3 < PF_3 < P(OMe)_3 < PMe_3 < PEt_3 < PPh_3 < PCy_3 < PtBu_3$$

An important and convenient aspect of phosphorous chemistry is the ability to monitor chemical reactions and to characterize phosphines and related systems via $^{31}P\{^1H\}$ NMR (I = ½) spectroscopy. Bonding and interaction with a metal center is usually accompanied by a significant coordination induced shift (CIS) downfield with respect to the free ligand. Furthermore information about bonding mode, symmetry and isomerism within the complex can be obtained[10].

1.5   NO – A non-innocent ligand

The assignment of formal oxidation[11] states to the metal in transition metal complexes containing ligands such as Cl, NH_3, PR_3 or CN is generally uncontroversial and leads to a single designation. A small number of ligands (e.g. bipyridines or diimines) provide for ambiguities due to their unpredictable redox activity and different possible binding modes – they are termed redox non-innocent ligands[12].

Free nitric[13–15] oxide (NO) is a colorless gas. Its first recognizable synthetic route has been attributed to Johann Glauber (1604-1679) who observed its formation by reacting sulfuric acid and potassium nitrate. Due to its odd (15) number of electrons it exists as a radical and is therefore paramagnetic. In a molecular orbital picture (Fig. 5) the unpaired electron is located in a π-antibonding (π*) orbital which is the HOMO. The formal bond order in radical NO is therefore 2.5 and rationalizes the low affinity of dimerization to N_2O_2. The latter compound can only be isolated in a matrix at very low temperatures. The bond length of free NO in the gas phase is 1.154 Å.
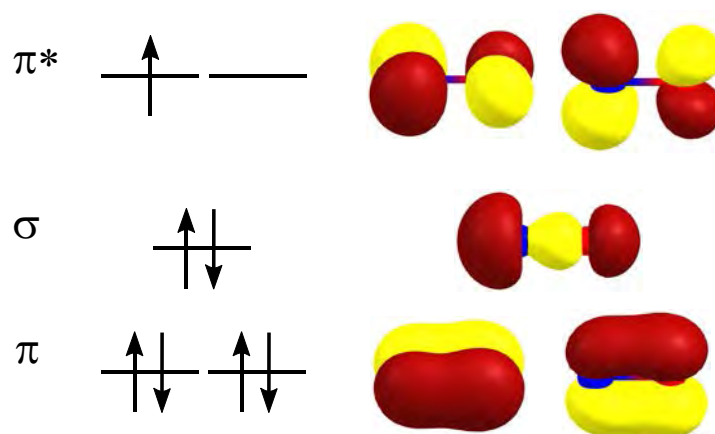

Fig. 5 Frontier orbitals of NO calculated at the RO-TPSS/6-31G* level of theory

A comparison of related diatomic molecules considering the *Aufbau* principle shows that N_2 and CO have the valence electron configuration $(\pi^*)^0$, NO $(\pi^*)^1$ and O_2 $(\pi^*)^2$ with a triplet ground state. In contrast to N_2 and O_2, the antibonding orbital of NO is not equally distributed but localized 60 % on the nitrogen and 40 % on the oxygen atom. NO can be oxidized to form the nitrosonium ion NO^+ and reduced to the nitroxyl ion, NO^-. Nitrosonium (also called nitrosyl) salts such as $NOBF_4$ or $NOSbF_6$ can be isolated and are commercially available.

NO is the prototype example of a non-innocent ligand able to bind to a metal center in structurally different modes, where the linear and the bent form can be seen as the extreme configurations. The linear nitrosyl can formally be viewed as a derivate of the nitrosyl cation, NO^+. This ion is isoelectronic to carbon monoxide, CO and therefore bonding between a nitrosyl ligand and a metal follows the same principles as the bonding in carbonyl complexes. The linear M-NO unit consists mainly of σ-donation from an occupied σ-orbital on the NO unit to an empty d-orbital of the metal center and of back-donation, which occurs by the interaction of two filled d-orbitals of π

symmetry with two orthogonal π-antibonding orbitals on NO. The bent nitrosyl is regarded as the two electron ligand NO⁻ isoelectronic to the diazenido (i.e iminonitrosyl) ligand –N=NR. In this case NO functions as an σ-donor and a single-faced π-donor. Fig. 6 depicts a simplified orbital interaction scheme for the linear and bent bonding mode in M-NO complexes.
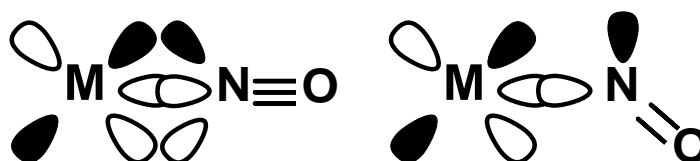

Fig. 6 Orbital interaction scheme for the linear and bent NO bonding mode

With an electron-deficient metal center, the linear nitrosyl prevails while the bent nitrosyl is more favored when the metal has a high d-electron count. This structural change can be viewed as an intramolecular redox process transferring electrons from the metal center to the NO unit. This process is responsible for the non-innocence of the NO ligand and explains why metal nitrosyl compounds are substantially different from equivalent metal carbonyl compounds. It should be noted that there are two further theoretical possibilities for bonding of NO to a metal center, namely as an isonitrosyl M-ON and as a side-on adduct. Furthermore, the Sulphur (thionitrosyls, M-N=S) and Selenium (selenonitrosyls, M-N=Se) analogs exist.

Complexes containing NO ligands are usually described or classified according to the bonding mode of the nitrosyl unit and the resulting M-N-O angle[A]:

    180° - 160°   linear (l)
    160° - 140°   intermediate (i)
    140° - 110°   bent (b)
    110° - 90°   π-bonded / side-on

Linear and bent NO ligands can be distinguished using Infrared spectroscopy (IR). Linear M-NO groups absorb in the region 1900 – 1700 cm⁻¹, whereas bent nitrosyls

---

[A] A statistic of M-N-O angles extracted from the CCSD database can be found in the Appendix

absorb in the region approx. 1700 – 1500 cm^{-1}. These vibrational frequencies for the NO stretching mode reflect the differing bond orders in linear and bent nitrosyls and hence the difficulties in assigning of a bonding mode.

To overcome the oxidation state ambiguities for NO as a non-innocent ligand, Enemark and Feltham[16] developed a widely adopted notation, which made no assumptions concerning the formal oxidation state of the metal center.

In this notation the electrons occupying the π* orbitals of NO are added to the d-electron count of the remainder of the complex. This {MNO}^{x} notation, where x is the total electron count, is always consistent no matter how the NO ligand(s) are treated. To illustrate its use, the formal d-electron count for the complex [Mn(CN)$_5$(NO)]$^{3-}$ is explained. Assuming that the CN ligands behave as normal spectator ligands and are associated with a charge of -1, the charge on the {MnNO} unit is +2. Since Mn^{2+} has 5 d-electrons and neutral NO has one electron in the π* orbital, the total electron count is 6, i.e. it's a {MnNO}^{6} complex.

1.6   Overview of known nitrosyl complexes

One of the earliest examples of nitrosyl compounds to be synthesized and isolated was sodium nitroprusside, Na$_2$[Fe(CN)$_5$NO] by Lionel Playfair in 1848. Nitroprusside[17] adopts an octahedral geometry with nearly perfect C$_{4v}$ symmetry. The M-NO group is almost linear (Fe-N-O angle of 176°) and leads to a stretching mode at ν(NO) = 1947 cm^{-1}. Accordingly, the NO ligand can be described as NO$^+$ and the oxidation state of the iron center can be assigned to +II. Further representative and related compounds are Roussin's[18,19] red and black salts; both belong to the biologically important class of iron-sulfur clusters (Fig. 7). Roussin's red salt anion can be described as edge sharing tetrahedrons, wherein a pair of Fe(NO)$_2$ units are bridged by a pair of sulfide ligands. The Fe-NO bonds are close to linear (NO$^+$) and each iron within the diamagnetic complex is assigned the oxidation state of −I. Roussin's black salt is structurally more complex. The [Fe$_4$(NO)$_7$S$_3$]$^-$ anion shows an incomplete cubane geometry and has point group symmetry C$_{3v}$. It can be constructed of one {FeNO}^{7} and three {Fe(NO)$_2$}^{9} units
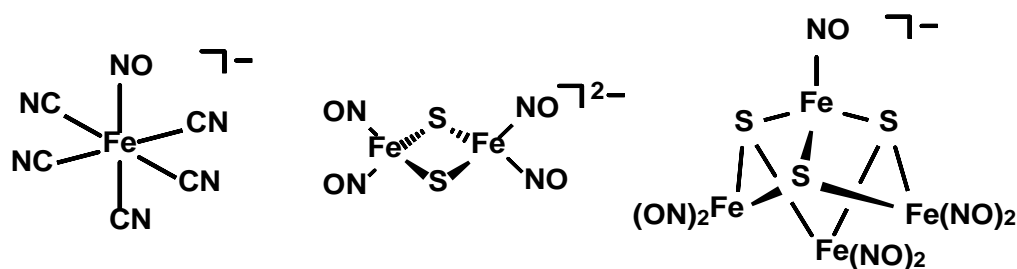
Fig. 7 Structural view of the nitroprusside ion (left), Roussin's red (middle) and black (right) salt anion.

In

contrast to metal carbonyls there are just a few homoleptic metal nitrosyls. These include $[M(NO)_4]$ (with M = Cr, Mo, W), $[Co(NO)_3]$, $[Rh(NO)_3]$ and $[Ir(NO)_3]$. The iron homoleptic tetranitrosyl complex $[Fe(NO)_4]^-$ provides for a special case[20]. It can be best described as a $\{Fe(NO)_2\}^9$ motif (having two linear NO groups, Fe-N-O ~ 161°) coordinated by two bent nitroxyl (NO^-, Fe-N-O ~ 107°) ligands. Regarding iron, there are numerous small nitrosyl complexes, such as $[Fe(CO)_3(NO)]^-$ and $[Fe(CO)_2(NO)_2]$ reported by Hieber[21] or halogenonitrosyl compounds such as $[FeX_2(NO)_2]^-$ (X = Cl, Br) reported by Connelly *et al*[22].

As mentioned in the previous section, coordinated NO can occur in various binding modes, i.e. (primarily) linear and bent. As in carbonyl complexes, bridging can also occur in NO complexes. Fig. 8 depicts one of the few examples of a μ^2 chromium complex[23], i.e., $[Cr(\eta^5\text{-}C_5H_5)(NO)(\mu^2\text{-}NO)]_2$ or shorter $[CpCr(NO)_2]_2$. This complex is isostructural to its analogous bridged iron carbonyl complex $[CpFe(CO)_2]_2$.
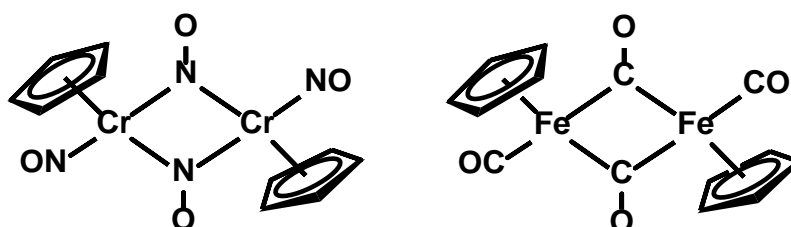

Fig. 8 Structural view of a bridged nitrosyl and isostructural carbonyl complex

Fig. 9 shall present a few examples of reported stable heteroleptic transition metal nitrosyl complexes throughout the periodic system. An extensive review of NO

complexes and their chemical reactivity has been given by Hayton and Legzdins[24]. NO complexes of early transition metals (groups III and IV) are virtually unknown. The majority of reported compounds are based on group VI to VIII metals. Nitrosyl complexes based on pincer ligands are reviewed in section **1.8**.
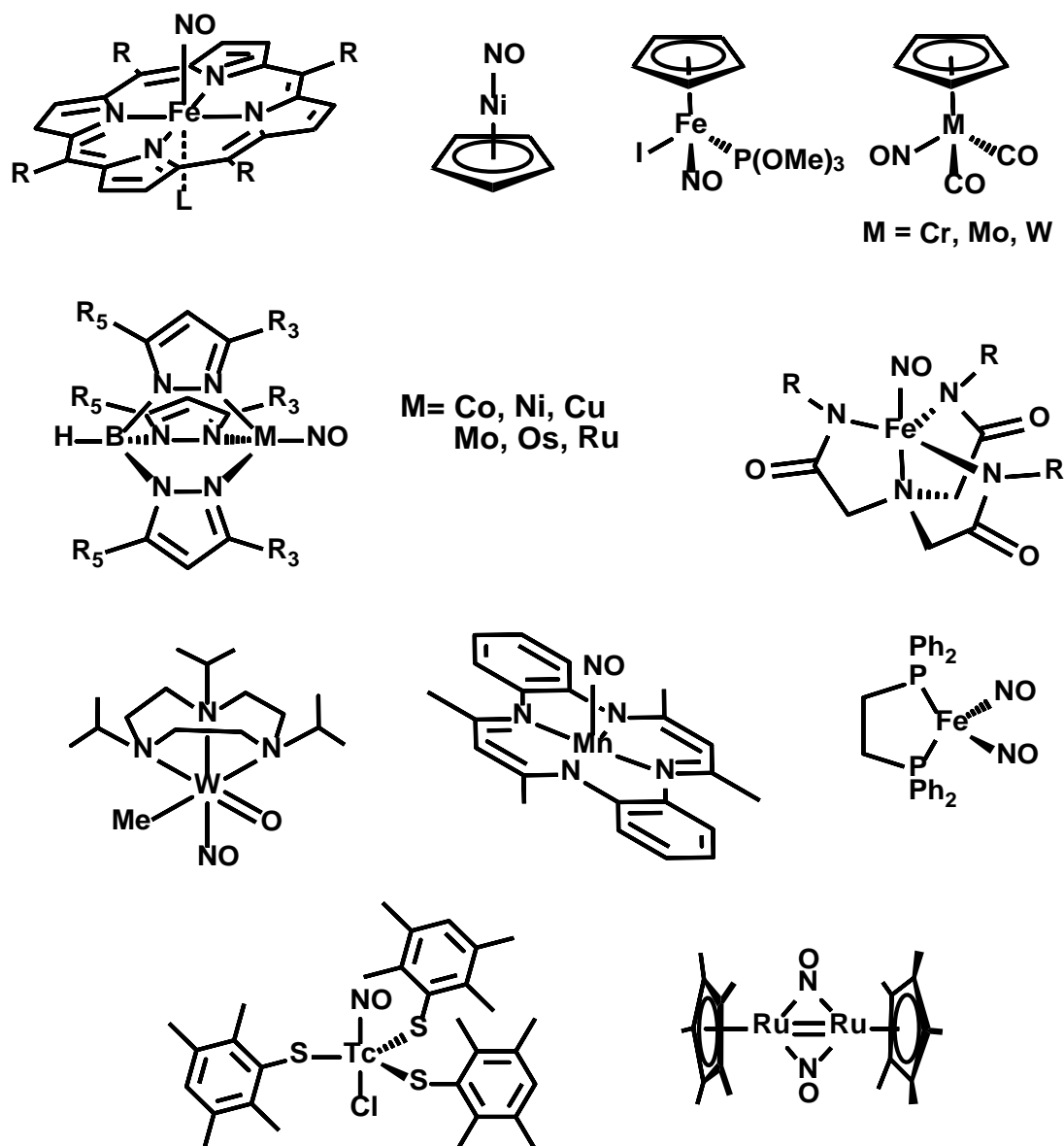
Fig. 9 Overview of known transition metal NO complexes based on Porphyrine, Cyclopentadiene (Cp), Scorpionate as well as bi- and tridentate ligands

1.7   Synthetic approaches towards NO complexes

In contrast to CO complexes, nitrosyl compounds can be prepared by numerous means and reagents. Extensive collections of preparatory methods have been given by Caulton[25], Legzdins[26] and Mingos.[27] The following section briefly summarizes all popular methods and approaches.

Nitric oxide / NO. Passing nitric oxide (NO) through a solution of a coordinatively unsaturated transition metal complex is the most convenient approach to prepare nitrosyl compounds. Since NO contains an unpaired electron this method can be applied to open shell paramagnetic starting materials; hence this way can be used to gain diamagnetic compounds.

$$[CoCl_2(PPh_3)_2] \xrightarrow{\text{NO}} [CoCl_2(NO)(PPh_3)_2]$$

$$V(CO)_6 \xrightarrow{\text{NO}} [V(CO)_5(NO)]$$
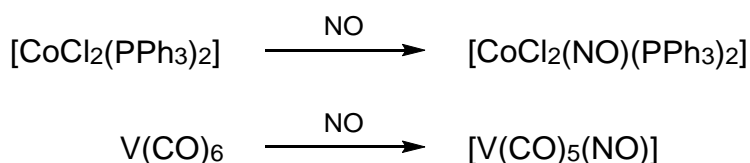
Nitrosonium salts / NO⁺. Addition or substitution reactions with nitrosonium sources such as $NOBF_4$ or $NOSbF_6$ provide a further convenient way to prepare metal nitrosyl complexes. A possible side reaction using the nitrosonium ion with low valent transition metal compounds can be a one electron oxidation of the complex with the evolution of gaseous nitric oxide.

$$[Ir(CO)(PPh_3)_2Cl] \xrightarrow{\text{NOBF}_4} [Ir(CO)(NO)(PPh_3)_2Cl][BF_4]$$
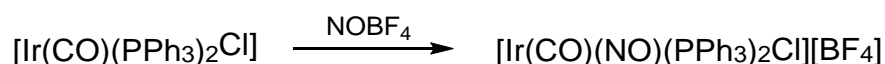
Nitronium salts / NO₂⁺. A more exotic but commercially available nitrosylation and nitraton agent is the stable nitronium ion. Various stable salts such as $[NO_2]BF_4$, $[NO_2]ClO_4$ or $[NO_2]PF_6$ can be isolated.

$$[CpRe(CO)_3] \xrightarrow[\text{- CO}_2]{\text{NO}_2\text{PF}_6} [CpRe(CO)_2(NO)][PF_6]$$
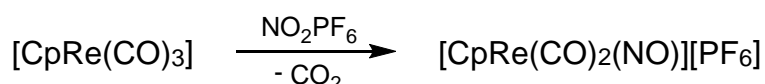
**Nitrite salts / NO$_2$⁻.** Nitrites such as NaNO$_2$ or AgNO$_2$ can be equally used to prepare nitrosyl (NO) as well as nitrito (NO$_2$) complexes.

$$Fe(CO)_5 \xrightarrow{\text{NaNO}_2} Na[Fe(CO)_3(NO)]$$

$$Na[Co(CO)_4] \xrightarrow{\text{NaNO}_2} [Co(CO)_3(NO)]$$
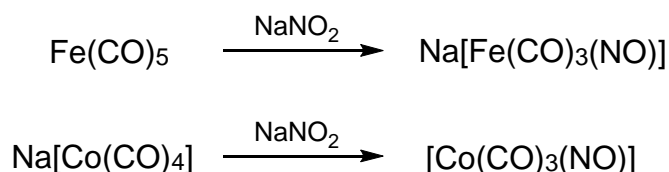
Other methods. A versatile agent for nitrosylation is N-methyl-N-nitroso-p-toluenesulfonamide, commonly referred to as Diazald™. This compound can be used as a safe precursor to diazomethane (CH$_2$N$_2$) as well as a NO source in inorganic chemistry. Another approach involves the reaction with nitrosyl halides such as NOCl which often proceeds via oxidative nitrosylation. The use of simple nitrosyl precursor compounds for ligand exchange reactions is another convenient way to prepare NO complexes.

$$[HMn(CO)_5] \xrightarrow{\text{Diazald}} [Mn(CO)_4(NO)]$$

$$[V(\eta-C_5H_5)_2] \xrightarrow{\text{NOCl}} [V(\eta-C_5H_5)_2Cl(NO)]$$
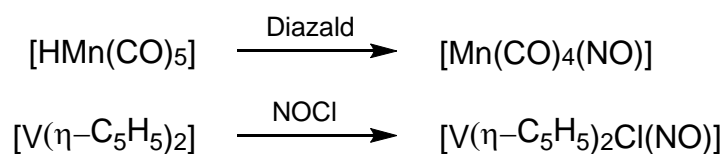
1.8 Nitrosyl pincer complexes

There are only few representatives of the class of pincer complexes bearing NO as a ligand. Rhodium complexes based on aromatic PNP and PCP pincer ligands as well as analogous PNP[28] systems with Ruthenium were reported by Milstein.

The preparation of the Rhodium(III) nitrosyl complex **II** was achieved by reaction of [Rh(PNP^{CH2}-tBu)Cl] **I** with NOBF$_4$ in acetone or alternatively by a twostep synthesis by reacting the same compound with AgBF$_4$ and subsequently with NO gas (Fig. 10). This work was later extended to Rhodium PCP[29] complexes such as [Rh(PCP^{CH2}-tBu)(NO)][BF$_4$] and derived systems thereof.
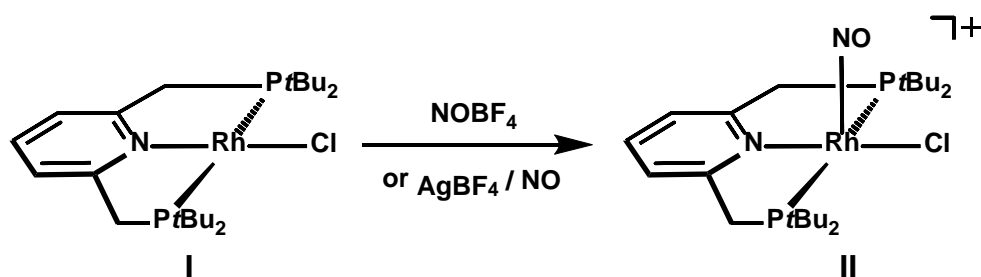
Fig. 10 Preparation of [Rh(PNP^{CH2}-tBu)(NO)Cl]

Analogous ruthenium complexes were prepared by Fogler[30] *et al.* in 2013 by reacting the same PNP^{CH2}-tBu ligand with the nitrosyl precursor RuCl$_3$(NO)(PPh$_3$)$_2$ in Ethanol. They obtained the octahedral Ru(II) complex **III** which was then transformed *via* the Ru(0) species [Ru(PNP^{CH2}-tBu)(NO)]$^+$ to compound **IV** (Fig. 11).
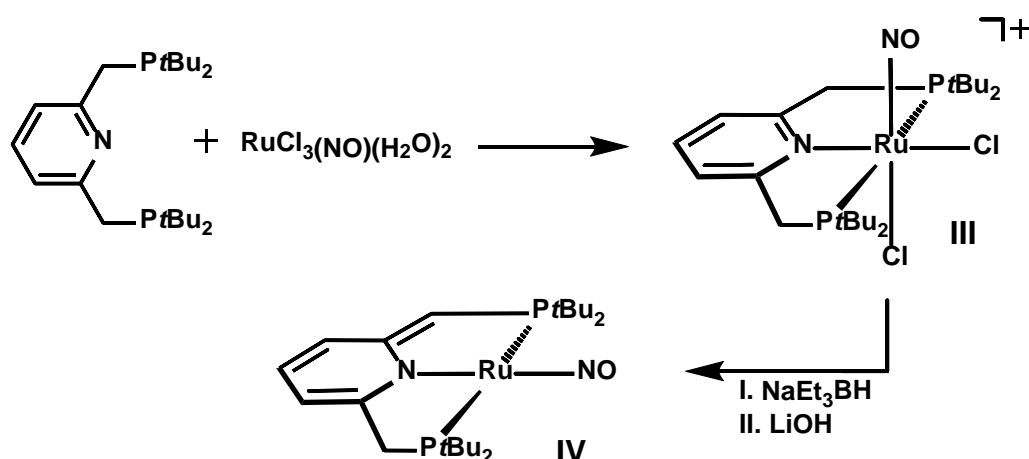
Fig. 11 Preparation of [Ru(PNP^{CH2}-tBu)(NO)Cl$_2$] and [Ru(PNP^{CH2}-tBu)(NO)]

Rhenium complexes based on aliphatic PNP pincer ligands were prepared and characterized by Choualeb[31] *et al.* Their synthetic approach was based on the reaction of the rhenium precursor pentabromonitrosylrhenate(II) with the ligand in Ethanol and subsequent treatment with LiEt$_3$BH in THF. The monohydride complex **V** was then reacted with KOtBu in THF to get [Re(N(C$_2$H$_4$PiPr$_2$)$_2$)(NO)(H)] and then with hydrogen H$_2$ to obtain the dihydro species **VI** (Fig. 15).

Fig. 12 Preparation of [ReN(C₂H₄P*i*Pr₂)₂(NO)(H)] and [ReN(C₂H₄P*i*Pr₂)₂(NO)(H)₂]

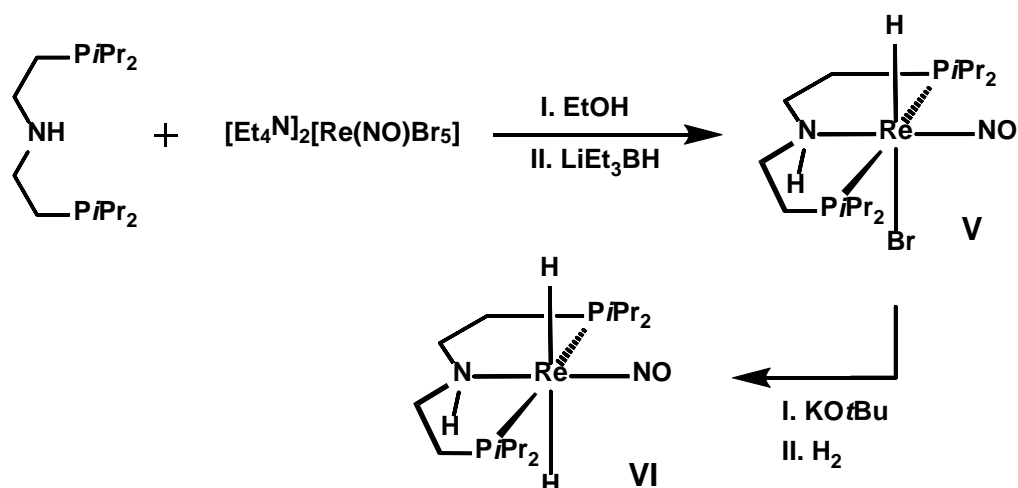Recently, the preparation and isolation of an iron pincer nitrosyl complex was achieved by Tondreau *et al.*[32] The reported compound **VIII** was prepared by treatment of the known mono carbonyl complex **VII** with AgNO₂ in THF (Fig. 13). The reaction proceeds via disproportionation of the Fe(II) initial starting material and therefore leads to the formation of two related iron species.
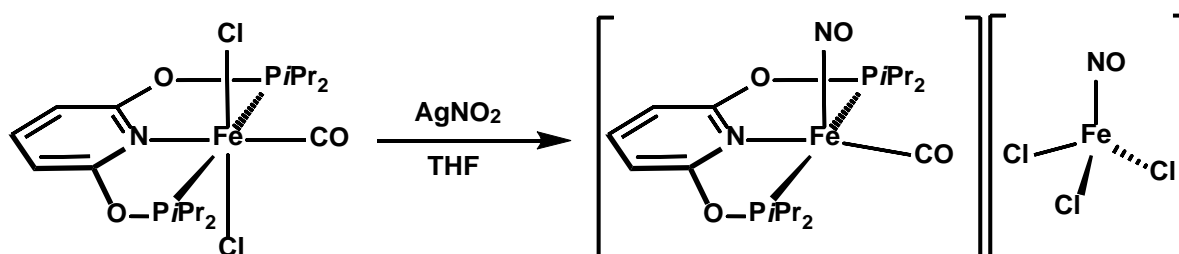
Fig. 13 Preparation of [Fe(*i*Pr-PONOP)(CO)(NO)][Fe(NO)Cl₃]

1.9 Low valent iron pincer complexes

In inorganic and organometallic compounds iron can in general be assigned a formal oxidation numbers between 0 and +VI. The most common oxidation states are +II and +III. In a few exceptional cases, the oxidation number can also be 0 or +I. Such compounds are termed low valent and require either neutral (CO) or positively charged (NO⁺) ligands attached to the metal center.

Regarding iron pincer complexes there are only a few examples of such compounds. In 2006 Chirik[33] and Goldman[34] independently reported the successful preparation and characterization of the Fe(0) dicarbonyl compounds **IX** and **X** (Fig. 14). Both compounds can be obtained from [Fe(PNP^{CH}-iPr)Cl$_2$] and [Fe(PNP^{CH}-tBu)Cl$_2$] by Na/Hg reduction under CO atmosphere. Although chemically related to each other, these two closed shell (S = 0) compounds proved to be very different in their spectroscopic (IR and NMR) behavior. In addition, Caulton[35] and Werner[36] reported structurally related Fe(I) compounds **XI** and **XII** based on anionic pincer ligands. These two complexes are based on the N(tBu$_2$PCH$_2$SiMe$_2$)$_2$ and a pyrrole derived PNP ligand. Both compounds were obtained in a similar fashion as described above, i.e. by KC$_8$ reduction of [Fe(PNP)Cl] under CO atmosphere. In contrast to the Fe(0) compounds, the latter ones are open shell species with a doublet ground state (S = 1/2) and a d^7 configuration.
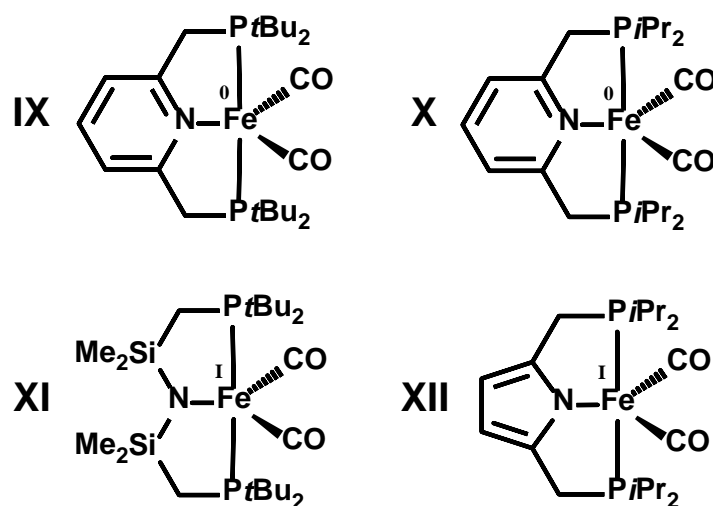
Fig. 14 Overview of low valent iron pincer complexes

1.10   Catalytic applications of nitrosyl complexes

Transition metal compounds bearing nitrosyl ligands do not yet play a significant role in homogeneous catalysis yet. Except for the biological and bioinorganic area, the catalytic potential of transition metal nitrosyl compounds is relatively unexplored, despite the fact that the NO ligand itself may possess various unique functions.

Due to its non-innocent character[37] the NO ligand is capable of serving as a strongly bound ancillary ligand functioning mainly as a two or three electron donor, providing for a temporary vacant site *via* electron transfer and the NO^+ / NO^- transformation (*vide supra*) and acting as a reversible oxygen source.

Reported catalytic applications (Fig. 15) of transition metal nitrosyl (NO) complexes include hydrogenations of alkenes[38] and nitriles, dehyrogenative silylation[39], allylic substitution reactions and carbonyl activation.[40]
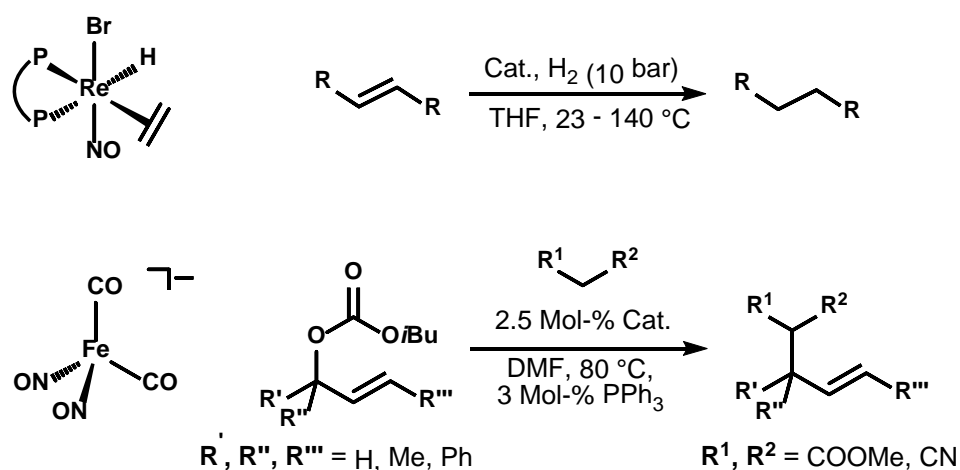
Fig. 15 Examples for reactions catalyzed by NO complexes

1.11   Computational aspects of nitrosyl complexes

With the advent of faster computers and more efficient and accessible software packages, computational studies of transition metal complexes have become a common complement to experimental research. The aim of all theoretical studies is to solve the Schrödinger equation $H\Psi = E\Psi$ for a multi electron system, with **H** being an appropriate Hamilton Operator and Ψ a solution (the wave function). Solving such an equation exactly is not possible except for the simplest systems and therefore approximate methods such as Hartree-Fock (HF), Density Functional Theory (DFT) and various post-HF methods (MP2, CI, CC) were developed. Today the most important and computationally most efficient method to describe transition metal complexes is Density Functional Theory[41].

Due to the non-innocent character of the NO ligand (vide supra) and its various bonding modes a thorough theoretical description of nitrosyl compounds and an

assignment of a formal oxidation state can be challenging. A simple single determinant picture as provided by standard HF or DFT theory is often inferior and therefore a high level *ab initio* treatment (i.e CAS-SCF) or a broken spin symmetry (BS) DFT approach can be necessary. Such BS solutions describe antiferromagnetic coupling within open-shell systems.

For instance, the {CoNO}^{9} compound[42] Tp*Co(NO) (Tp* = hydro-tris(3,5-Me$_2$-pyrazolyl)borate) (Fig. 16) with an experimentally determined S = 1/2 ground state and an nearly linear (173.5°) Co-N-O group is best described by a BS solution where a Co(II) / S = 3/2 metal center is coupled to a triplet NO$^-$ / S = 1 anion. A multi-configurational CAS-SCF calculation on the same geometry corroborates the DFT results. Using an extended Enemark-Feltham notation, this complex can described as {L$_3$Co^{II}(NO$^-$) (S = 1/2)}^{17} with 17 being the number of valence electrons.
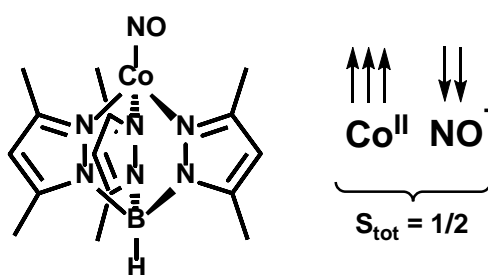
**Fig. 16 Molecular structure and
proposed spin coupling for Tp*Co(NO)**

1.12   Literature

Besides all quoted scientific publications (primary sources) throughout this work there is a number of recommendable reviews and books on NO chemistry. This literature can be used to gain an overview of nitrosyl systems in inorganic, organic, bioorganic and theoretical chemistry as well as catalysis.

Reviews:

Introduction: Nitric Oxide Chemistry
Chem. Rev., **2002**, *102*, 857–860.

Coordination and Organometallic Chemistry of Metal−NO Complexes
Chem. Rev., **2002**, 102, 935−991.

Books:

Nitrosyl Complexes in Inorganic Chemistry, Biochemistry and Medicine I
D. Michael, P. Mingos, Springer (Editor), Springer, 2014

Nitrosyl Complexes in Inorganic Chemistry, Biochemistry and Medicine II
D. Michael, P. Mingos, Springer (Editor), Springer, 2014

Nitrosation Reactions and the Chemistry of Nitric Oxide
D. L. H. Williams, Elsevier, 2004

2   Results and Discussion

The few Ruthenium based nitrosyl pincer complexes reported (*vide supra*) prove that octahedral or quadratic pyramidal NO complexes of group XVIII transition metals should in general be feasible by preparative methods or at least thermodynamically stable. Although CO and NO^+ are formally isoelectronic and octahedral iron carbonyl complexes are easily prepared by reacting $[Fe(PNP)X_2]$ with CO in solution, there are no reports on analogous (Fig. 17) iron nitrosyl compounds
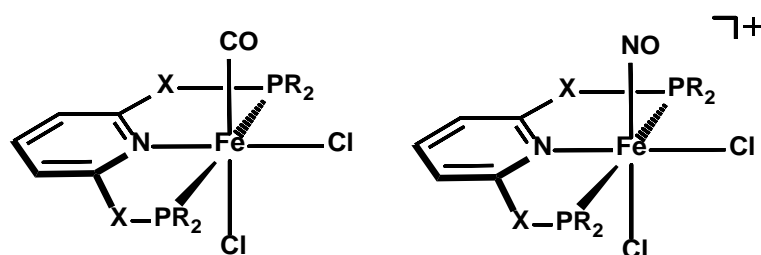
Fig. 17 Analogous iron carbonyl and nitrosyl complexes

Upon treatment of **1a** with nitrosyl $NOBF_4$ in dry DCM at low temperatures (- 20 °C) the paramagnetic purple colored compound **2a**·BF_4 is formed (Fig. 18). The formation of the Fe-NO bond is clearly visible in the infrared spectrum, showing one strong absorption band at $v(NO) = 1747$ cm^{-1}. This wave number can be ascribed to an N-O stretching mode and its value is very indicative for a linear M-NO group.
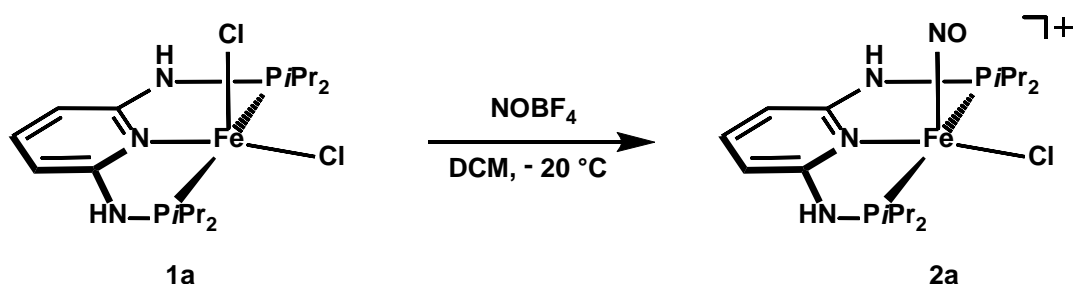
Fig. 18 Reaction scheme for the formation of [Fe(PNP- *i*Pr)(NO)Cl]BF$_4$

Contrary to expectations no octahedral complex is formed, but a disproportionation of the initial Fe(II) precursor into the paramagnetic target complex takes places giving yields less than 50 %. Due to the paramagnetism of the system, recorded ^1H NMR spectra exhibited only broad and featureless signals and $^{31}P\{^1H\}$ NMR as well as $^{13}C\{^1H\}$ NMR spectra exhibited no signals at all.

Assuming the iron atom within the molecule to have a d^7 configuration, two different spin states seem possible, a low spin state (S = 1/2) with one unpaired electron and a high spin state (S = 3/2) with three unpaired electrons. A measurement of the solution magnetic moment utilizing the EVANS method indicated a doublet ground state and hence a low spin configuration.

The solid-state structure of this complex was determined by X-ray diffraction. Suitable crystals were obtained by diffusion of pentane into a solution of the crude reaction product in THF. Compound **2a** crystalizes in the orthorhombic space group Pbcm as **2a**·BF_4 with one half of the target complex and one half of BF_4 in the asymmetric unit. A ORTEP representation of **2a** is depicted in Fig. 19 and selected bond lengths (Å) and bond angles (°) are given in the captions. The coordination geometry can be described as slightly distorted quadratic pyramidal with a geometry parameter of τ_5 = 0.32 (τ_5 = 0 describes a perfect quadratic pyramid). The PNP ligand is coordinated to the iron center in a typical tridentate meridional mode, with a P–Fe–P angle of 158.92(7) °. The complex cation shows C_S point group symmetry imposed by a mirror plane through Fe, N3, N1 and Cl. The nitrosyl group is in the apical position with a Fe-N-O angle of 161.4(6) ° strongly deviating from linearity. The bond lengths around Fe are Fe-P 2.2824(10) Å, Fe-Cl 2.2291(17) Å, Fe-N1 2.015(4) Å and Fe-N3 1.781(7) Å.

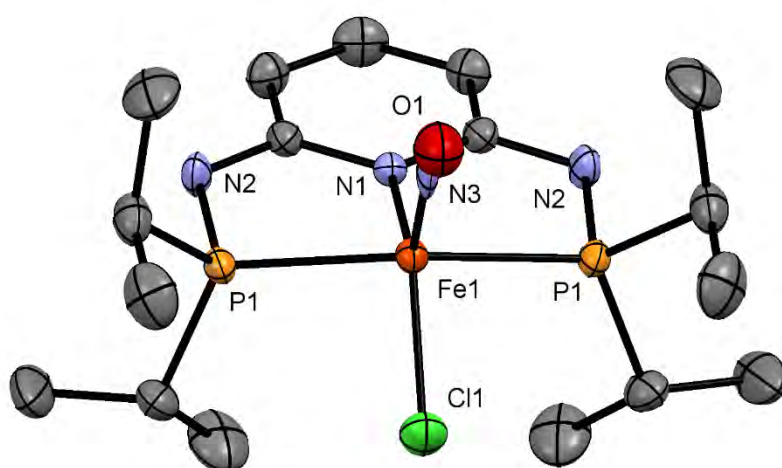**Fig. 19 Structural view of 2a showing 50% displacement ellipsoids (H atoms and BF$_4$ counter ion omitted for clarity). Selected bond lengths [Å] and angles [°]: Fe1-N1 2.015(4), Fe1-Cl1 2.2291(17), Fe1-N3 1.781(7), Fe1-P1 2.2824(10), P1-Fe1-P1 158.92(7), N3-Fe1-Cl1 105.24(19), N3-Fe1-N1 115.4(2), N1-Fe1-Cl1 139.37(13). Fe1-P1 and Fe1-P2 are equivalent by mirror symmetry**

To investigate the influence of the ligand on the reactivity towards nitrosyl salts, dihalide precursor complexes with the PNP^{Me}-iPr and the PNP-tBu ligand were used consecutively. The Reaction of **1b** with NOBF$_4$ (Fig. 20) under the same conditions as stated above yields the low spin complex **2b**·BF$_4$ having one strong absorption band at v(NO) = 1753 cm^{-1} and. Both **2a**·BF$_4$ and **2b**·BF$_4$ stand out by their remarkable stability towards air as compared to other known Fe(0) and Fe(I) iron complexes.

R = iPr, R' = Me   **1b**
R = tBu, R' = H   **1c**

R = iPr, R' = Me   **2b**
R = tBu, R' = H   **2c**
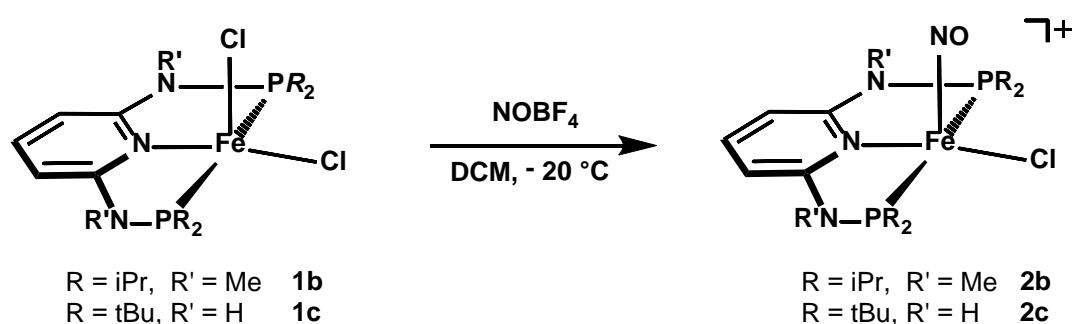
Fig. 20 Reaction scheme for the formation of [Fe(PNP^{Me}-iPr)(NO)Cl]BF$_4$ and [Fe(PNP-tBu)(NO)Cl]BF$_4$
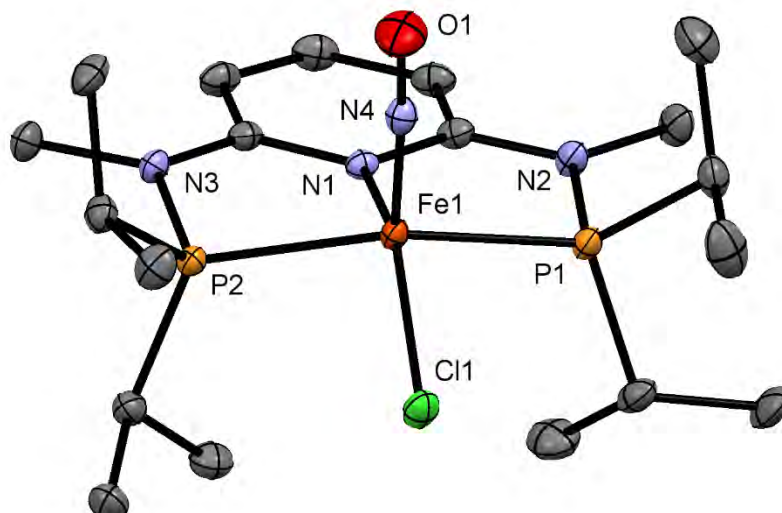
Fig. 21 Structural view of 2b showing 50% displacement ellipsoids (H atoms, counter ion and solvent molecules omitted for clarity). Selected bond lengths [Å] and angles [°]: Fe1-N1 1.9922(17), Fe1-Cl1 2.2613(6), Fe1-N4 1.6763(19), Fe1-P1 2.2599(6), Fe1-P2 2.2481(6), P2-Fe1-P1 157.66(3), N4-Fe1-Cl1 109.41(6), N4-Fe1-N1 106.59(8), N1-Fe1-Cl1 143.98(5).

The molecular structure of **2b** was confirmed by an X-ray diffraction study of single crystals obtained by slow diffusion of pentane into a concentrated solution of **2b**·BF$_4$ in THF at room temperature. Compound **2b**·BF$_4$ crystalizes in the orthorhombic space group Pbcn with one complex molecule, one BF$_4$ unit and one half of THF in the asymmetric unit. A ORTEP structural representation of **2b** is depicted in Figure 21 and selected bond lengths (Å) and bond angles (°) are given in the captions. The coordination geometry can be described by a geometry parameter of τ$_5$ = 0.23. The nitrosyl group is in the apical position with a Fe-N-O angle of 176.99(17) °. The bond lengths around Fe center are Fe-P1 2.2599(6) Å, Fe-P2 2.2481(6) Å, Fe-Cl 2.2613(6) Å, Fe-N1 1.9922(17) Å and Fe-N4 1.6763(19) Å.

Upon reaction of the analogous bromine precursor [Fe(PNP^{Me}-*i*Pr)Br$_2$] (**2a'**) with NOBF$_4$ in DCM the anticipated nitrosyl complex [Fe(PNP^{Me}-*i*Pr)(NO)Br][FeBr$_4$] (**2b'**·FeBr$_4$) is obtained. This ion pair formed during chemical reaction strongly supports the assumption of this process being a disproportionation. The initial Fe(II) compound is transformed into a cationic low valent Fe(I) nitrosyl complex and a Fe(III) counter ion (Fig. 22). The solid-state structure of **2a'** was determined by XRD and can be found in the Appendix.
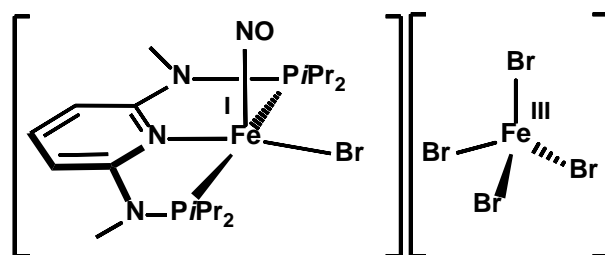
Fig. 22 Disproportionation products as ion pair

The reaction of **1c** however, a complex featuring a very bulky and sterically demanding ligand, with NOBF$_4$ in DCM yields a mixture of products. Single crystal XRD confirms unambiguously the formation of the corresponding cationic nitrosyl complex **2c** as well as it shows the formation of a side product wherein a BF$_4$ unit is directly coordinated to the complex center replacing the halide (see Appendix). Using another similar reagent, NOSbF$_6$, with the chemically very inert SbF$_6^-$ counter ion, the same target complex is formed directly with a NO absorption band at v(NO) =

1742 cm^{-1}. The solid-state structure of **2c**·SbF$_6$ was elucidated by X-Ray diffraction. The aforementioned compound crystalizes as a crystal twin in the triclinic space group P1 with one molecule of **2c** and 3/2 of the SbF$_6$ ion in the asymmetric unit.

A ORTEP representation of **2c** is depicted in Fig. 23 and selected bond lengths (Å) and bond angles (°) are given in the captions. The geometry index calculated from the bonding angles of the coordination polyhedron is τ$_5$ = 0.10.
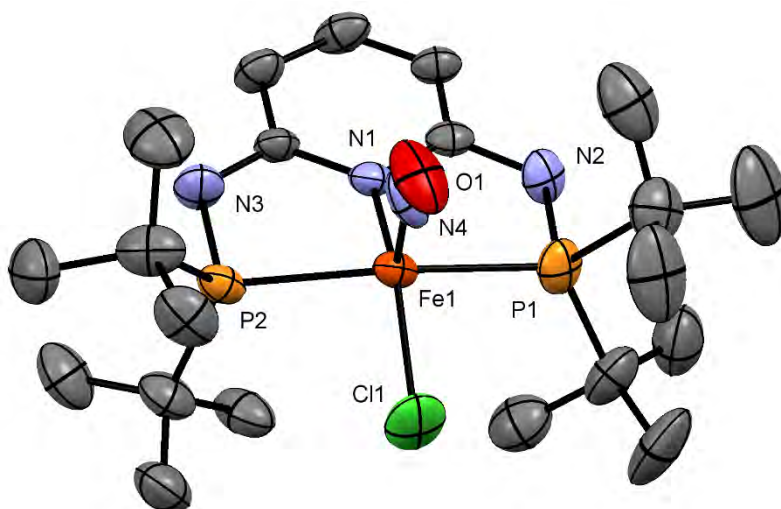
Fig. 23 Structural view of 2c showing 50% displacement ellipsoids (H atoms and solvent molecules omitted for clarity). Selected bond lengths [Å] and angles [°]: Fe1-N1 2.012(7), Fe1-Cl1 2.241(4), Fe1-N4 1.695(12), Fe1-P1 2.343(4), Fe1-P2 2.336(4), P2-Fe1-P1 157.81(14), N4-Fe1-Cl1 99.4(4), N4-Fe1-N1 108.7(5)

A comparison of **2a**, **2b** and **2c** regarding their molecular structure as determined by XRD and their spectroscopic properties shows that all three complexes have a distorted square pyramidal coordination geometry with geometry indices (τ$_5$) between 0.10 and 0.32, where τ$_5$ = 0 describes a perfect square pyramid and τ$_5$ = 1 a perfect trigonal bipyramid. The bonding angles for Fe-N-O lie between 161.4(6) ° and 176.99(17) ° and the {FeNO} moiety can be thus considered as nearly linear. The bond lengths for the N-O bond vary between 1.015(7) Å and 1.163(2) Å and similarly the Fe-N^{NO} bond lengths between 1.6763(19) Å and 1.781(7) Å. The wave numbers (IR) for the N-O stretching mode lie in a small interval between 1742 cm^{-1} and 1753 cm^{-1}. These metrical parameters and wave numbers indicate a very similar electronic structure in all three molecules described above. Both, the Fe-N and N-O bond lengths are comparable to literature known iron nitrosyl complexes: Boncella's[32]

Fe(0) complex [Fe(P^{O}N^{O}P-iPr)(NO)(CO)]$^+$ for instance, exhibits a bond length of 1.691(2) Å for the Fe-N and 1.164(3) Å for the N-O bond. The N-O absorption can be found at 1732 cm^{-1} in the IR spectrum. Likewise, Meyer's[43] Fe(I) nitrosyl complex [L^{TC}Fe(NO)]$^{2+}$ exhibits a bond length of 1.670(3) Å for the Fe-N bond, 1.166(4) Å for the N-O bond and a N-O stretching mode at 1748 cm^{-1}.

Computational study

To investigate the electronic structure and bonding situation of the previously described and characterized {FeNO}^{7} systems, DFT calculations where performed. The model compound **2a** was fully optimized at the U-TPSS/6-311G(d,p) level of theory for its doublet (S = 1/2) and quartet (S = 3/2) state without any symmetry constraints. Frequency calculations where performed to confirm the nature of the stationary point yielding no imaginary frequencies for both species. A DFT optimized structure of the low spin species on a full model agrees favorably with the metrical parameters of the experimentally (XRD) determined molecular structure of **2a**. It is noticed that DFT calculations converge the geometry of the low spin isomer into virtually C$_S$ symmetry, although the symmetry constraint is not imposed during optimization. Calculated bond lengths for the inner coordination sphere (i.e. Fe-N, Fe-P and Fe-Cl distances) have a root mean square deviation (RMSD) of 0.054 Å from the experimentally determined values. The same parameters calculated for the high-spin species differ significantly from the low-spin species and the XRD values. Calculated bond lengths, bond angles and uncorrected v(NO) for both species are summarized in Tab. 1.

Tab. 1 Bond lengths (Å), angles (°) and NO mode (cm^{-1})

Parameter	S = 1/2	S = 3/2
Fe-P1	2.265	2.480
Fe-N1	2.016	2.227
Fe-N3	1.663	1.708
Fe-Cl1	2.253	2.227
Fe-N-O	161.7	159.7
P-Fe-P	160.1	151.1
v(NO)	1793	1818

To explain the preference of the low spin state over the high spin state calculations of the relative spin-state energies where performed using various exchange-correlation

functionals and the 6-311G(d,p) basis set for all atoms. It is known that these results are highly dependent on the class of functional and the amount of exact exchange encoded in the functional. Thus TPSS (mGGA) and OPBE (GGA) yield doublet ground states favored by 15.4 (ΔG = 13.4) and 7.8 kcal·mol^{-1}, respectively. B3LYP (a hybrid with 20 % exact exchange) yields a quartet ground state favored by 1.9 kcal·mol^{-1} and TPSSh (the hybrid version of TPSS with 10 % exact exchange) gives a similar (7.3 kcal·mol^{-1}) result to OPBE. These energies were corrected by adding zero-point vibrational (ZPVE) energies. Overall the experimental findings (magnetometry and XRD) corroborate the computational results and highlights the challenge to calculate accurate spin state energies for iron nitrosyl systems using density functional theory[44].
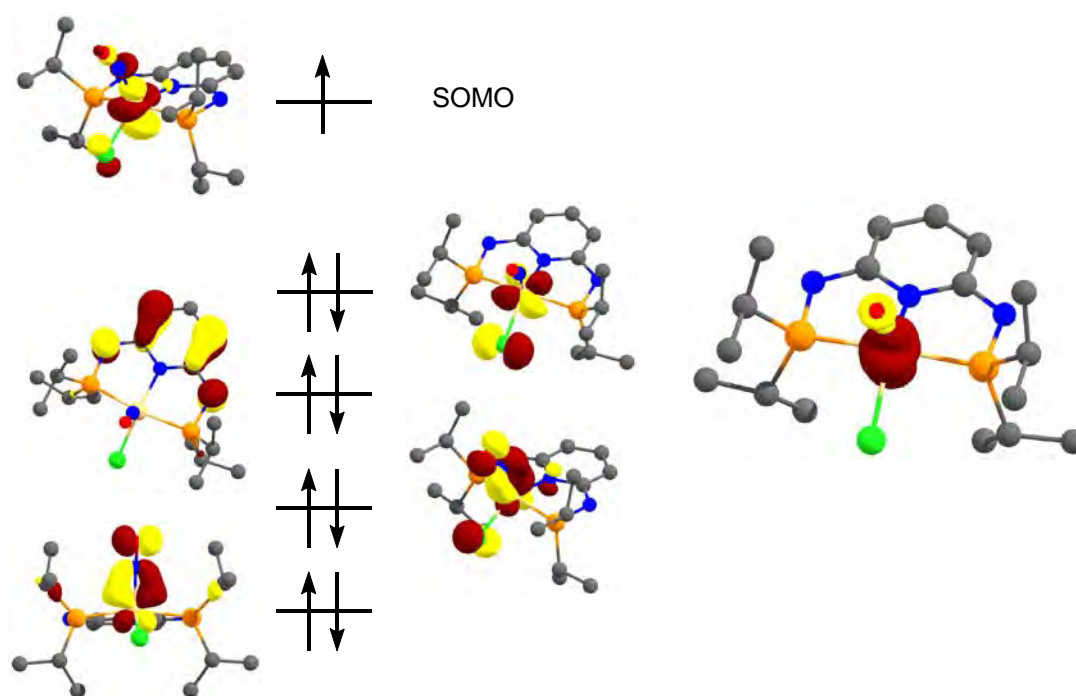
Fig. 24 Molecular orbital scheme (left) and spin density of 2a (right)

To gain further insight into the bonding situation and the ground state electronic structure of the obtained low spin (S = 1/2) complex, additional calculation were carried out using the ORCA 4.0 program package. To prove the validity of the spin-unrestricted Kohn-Sham DFT approach, unrestricted corresponding orbitals were calculated. A UCO analysis involves a unitary transformation of the canonical MOs to generate a set of α and β orbitals with maximum overlap.[45] An overlap value of one is considered to be a covalent interaction, whereas orbital pairs with overlap values

significantly less than one (< 0.85) are considered magnetic orbitals. Overlap values of zero are obtained for singly occupied orbitals. By this means it can be shown that there is a perfect match between all α and β orbitals leaving one singly occupied orbital (SOMO, zero overlap) unmatched. Furthermore, the spin contamination of the KS wave function, as seen by inspection of the expectation value of the S^2 operator, is small. The deviation from the theoretical value of $S(S+1) = 0.75$ is only 0.02. Both results indicate that the UHF wave function is valid and no broken-symmetry solution or magnetic coupling has to be considered. Quasi restricted orbitals (QROs) where then generated to produce a more familiar and intuitive scheme in terms of doubly and singly occupied orbitals (Fig. 24, left). The SOMO (HOMO) can be identified as an iron centered d_{z2} orbital and the HOMO-1 as an iron d_{xy} orbital. This assignment is in accordance with a simple ligand field picture for a square pyramidal geometry and a d^7 low spin configuration. The numerical value for the spin density on the iron center is 1.00 and -0.07 for the NO unit supporting the interpretation of NO being formally a NO^+ ligand.

Localized molecular orbitals were computed by the Pipek-Mezey localization procedure to obtain a comprehensible picture of the bonding interaction between Fe and the NO unit. Fig. 25 depicts three LMOs that describe one σ- and two π-bonds. Consecutively, the Mayer-Wiberg bond order (index) for the Fe-NO interaction is 1.26 and 1.59 for the N-O interaction.

Fig. 25 Localized Orbitals describing the σ- and π-bonds in 2a

Alternative approaches

The formation of these nitrosyl complexes by reaction with $NOBF_4$ or $NOSbF_6$ in DCM exhibits several drawbacks and disadvantages. The overall chemical reaction is a disproportionation, wherein the starting compound is transformed into the target complex and unknown Fe(III) compounds, following the equation 2 Fe(II) → Fe(I) +

Fe(III). Therefore at least half of the starting material is lost and formed Fe(III) residues are very difficult to completely separate from the target product.

Treatment of the same [Fe(PNP)X$_2$] precursor complexes (X = Cl, Br) with NO gas in dry methanol (or isopropanol) at room temperature leads surprisingly to the direct formation of the very same complexes as described above (Fig. 26). This reaction however does not proceed via disproportionation and thus any loss of substance. From the theoretical point of view, a formal analogy should be the reaction of [Fe(PNP)X$_2$] with CO. This known reaction however transforms the initial substance into a octahedral low-spin (S = 0) complex of the general form [Fe(PNP)(CO)X$_2$].
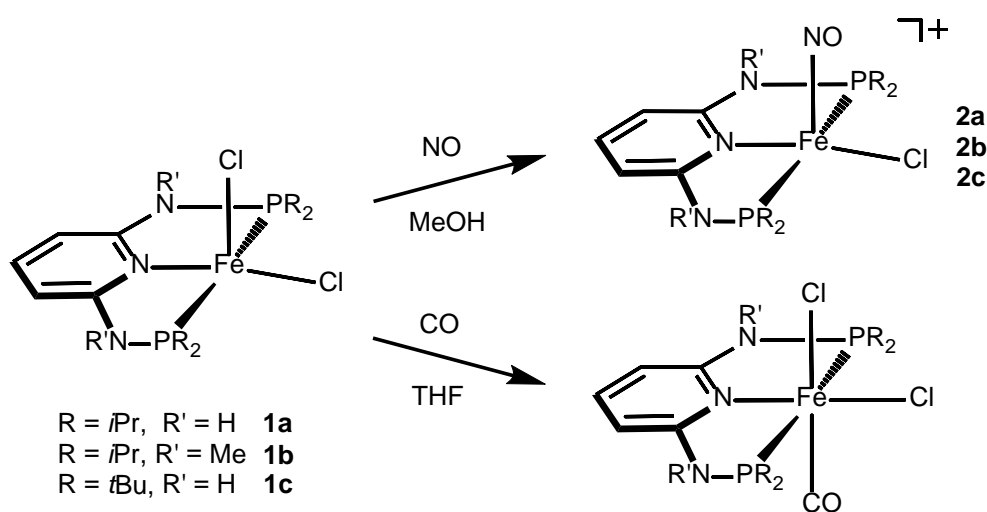
Fig. 26. Scheme for the reaction of [Fe(PNP)Cl$_2$] with NO and CO

All compounds formed by reaction with NO gas where characterized both by means of IR spectroscopy and mass spectrometry. A comparison of MS spectra of these compounds and data acquired for the reference compounds prepared above showed excellent agreement. In the same manner the (solid state) ATR-IR spectra, especially the wave numbers for ν(NO) and the fingerprint region, where in compliance with reference material.
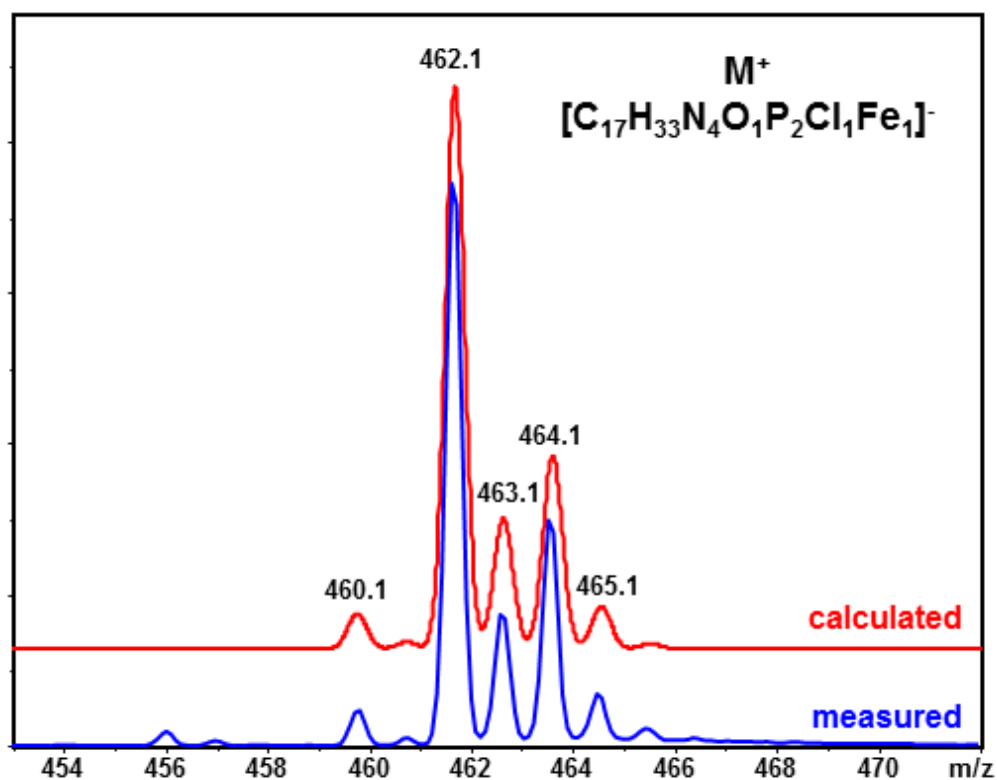
Fig. 27 ESI-MS Spectrum of 2a·Cl in MeOH

Therefore, in the full scan (positive ion-mode) ESI-MS spectrum of **2a**·Cl (in MeOH) only signals at m/z 461.8 (Fig. 27) and 431.9 were recorded. The first peak can be ascribed to the intact cationic species [Fe(PNP-*i*Pr)(NO)Cl]$^+$ while the latter, differing by m/z = 29.9, can be explained by NO loss of the initial complex. In the MS/MS spectrum of the M$^+$ peak this fragmentation pattern is observed as well and furthermore very characteristic for all prepared iron nitrosyl complexes in general.

It is noteworthy that the reaction of NO with **1a** – **1c** in different solvents than alcohols (i.e. DCM or THF) leads to the formation of two or three major products as evidenced by IR spectroscopy.

Fig. 28 X-band EPR Spectrum of 2aCl in DCM
Magnetic field (G)
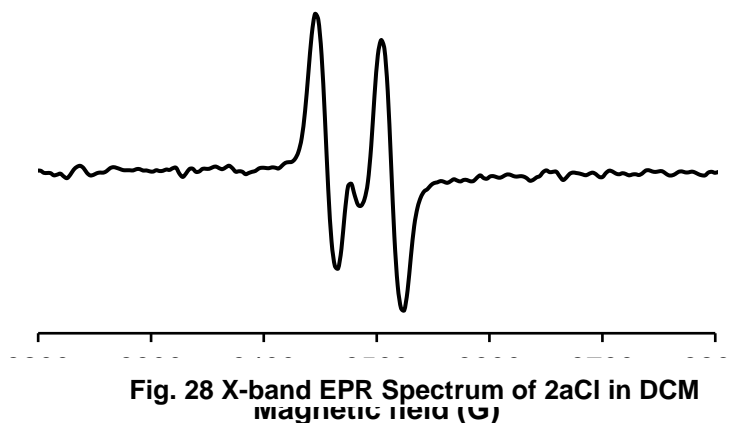
Alongside Mass Spectrometry (MS) and Infrared Spectroscopy (IR), two methods used to characterize the reaction products, Electron Paramagnetic Resonance spectroscopy (EPR or ESR) was applied to investigate compound **2a**·Cl in solution. Fig. 29 displays an X-Band EPR Spectrum of **2a**·Cl in DCM (100 µM) at room temperature. The splitting of the lines occurs due to hyperfine interaction of the unpaired electron with the iron nucleus (I = 0). Contrary to expectations not only one single S = 1/2 compound is found in the sample, but two closely related ones. The [57]Fe Mössbauer spectrum (Fig. 29) of solid **2a**·Cl and **2b**·Cl supports this assumption by proving the presence of two similar Fe(I) compounds in both compounds. The values of the hyperfine parameters obtained from fitting two quadrupole doublets to the experimental spectra are presented in the Appendix. A SQUID magnetometric measurement of these two samples gives an effective magnetic moment of 2.2(1) µB (see Appendix).
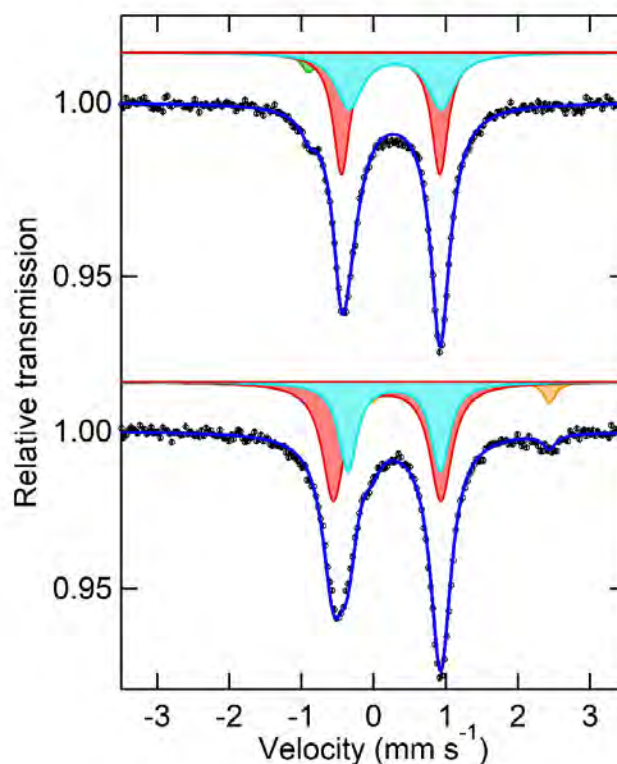
Fig. 29 Mössbauer Spectra collected at 78 K for solid 2a·Cl (upper spectrum) and 2b·Cl (lower spectrum)

These experimental findings could be explained if assuming that two different structural isomers are formed in the reaction between the precursor (**1**) and gaseous nitric oxide. Fig. 30 depicts a simplified description of the reaction mechanism. Initially, the coordinatively unsaturated high spin (S = 2) complex [Fe(PNP)Cl$_2$] (with quadratic pyramidal geometry) reacts with NO$^\bullet$ (radical, S = 1/2) to an octahedral intermediate [Fe(PNP)(NO)Cl$_2$] (either S = 3/2 or S = 1/2). Analogously to the known reaction[46] of CO towards **1** in solution, *cis* and *trans* isomers of the intermediate (***cis*-IM** and ***trans*-IM**) are likely to be formed. A glance at the DFT optimized structures of the possible intermediates (*cis* and *trans*, low and high spin) shows a substantial increase in the Fe-Cl bond lengths (> 2.4 Å) as compared to the target complex (**2**) or the precursor. A simulation of implicit solvation effects via the Polarizable Continuum Model (PCM, MeOH) leads to a further increase of the Fe-Cl bond lengths during geometry optimization. This supports the idea of a rather weak bond and easy dissociation of **IM** to the cationic form. Therefore another possibility regarding isomerism is the existence of **2** with the nitrosyl group in the basal position as opposed to **2a**·BF$_4$ and its crystal structure (vide supra).
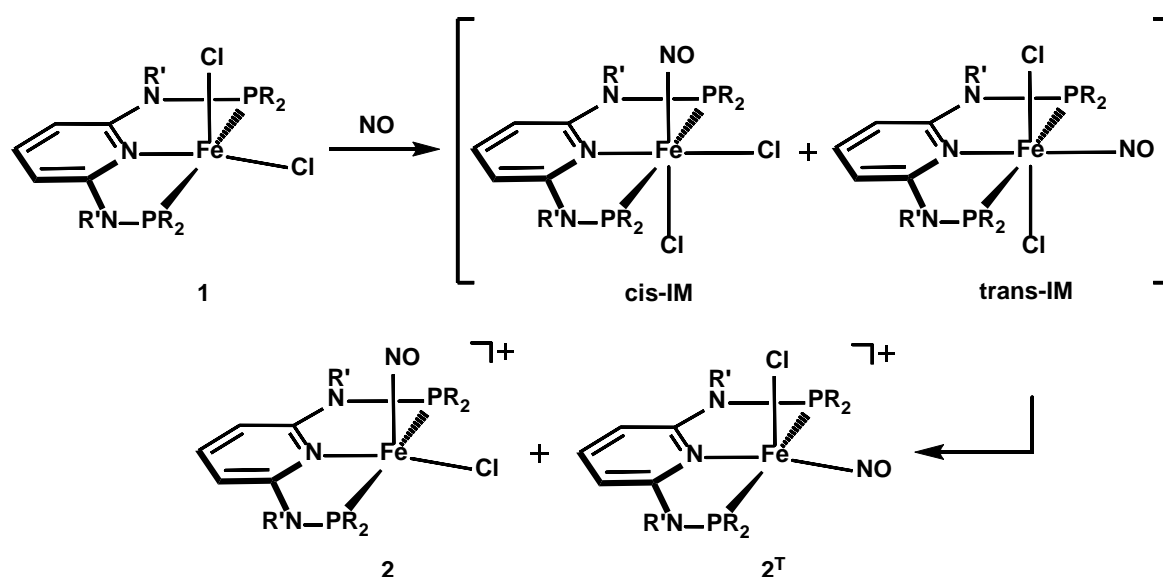
Fig. 30 Mechanistic description of the reaction between NO and [Fe(PNP)Cl₂] in solution

Both **2** and **2^T** are structural isomers and would likely be identical upon analysis by MS but slightly different in their behavior towards ^{57}Fe Mössbauer- and EPR-Spectroscopy.

Upon reaction of **2a**·Cl with a halide scavenger such as AgBF$_4$ or AgOTf in DCM an exchange of the counter ion occurs and hence formation of **2a**·BF$_4$ or **2a**·OTf. The reaction is irreversible and yields a product with the same v(NO) in the IR spectrum as compared to reference substances.

Influence of other PNP ligands

The PNP-Ph ligand provides for a special case. Reaction of FeCl$_2$ with this ligand does not yield a pentacoordinated pincer complex (such as **1a** – **1c**), but the κ^2-κ^3 complex[47] [Fe(PNP-Ph)$_2$Cl]Cl (**1d**) with two pincer ligands attached to the metal center. This complex shows no reactivity towards NOBF$_4$ and only very slow reactivity towards NO gas yielding a partially decomposed product with a very weak absorption band at 1773 cm^{-1}. A alternative approach utilizing octahedral [Fe(PNP-Ph)(CO)Cl$_2$] did not succeed.

To compare the influence of the linking atoms within the pincer scaffold, iron precursors based on the PONOP-iPr and the PNP^{CH2}-iPr ligand were reacted with

NO$^+$ and NO$^•$ gas accordingly (Fig. 31). Reactions of both **1e** and **1f** with NOBF$_4$ in DCM at low temperatures or NO gas in MeOH yield dark red to purple solutions.

The nitrosyl complex **2e** shows a NO absorption band at v(NO) = 1767 cm^{-1} and **2f** at v(NO) = 1838 cm^{-1}. Both complexes turned out to be very sensitive towards air and quickly turned green upon exposure. Both compounds could neither be crystalized nor isolated in a pure form.
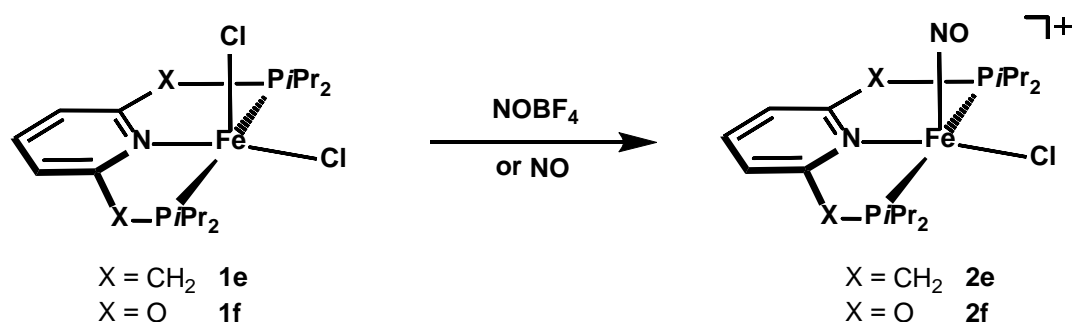
Fig. 31 Scheme for the Reaction of [Fe(PNP^{CH2}-*i*Pr)Cl$_2$] and [Fe(PONOP-*i*Pr)Cl$_2$] towards NO$^+$ and NO gas.

These two examples show the dramatic impact of the linking group X (X = CH$_2$, O, N) within the pincer scaffold. Whereas N linked systems (i.e. **2a**, **2b** and **2c**) proofed to be highly stable, both CH$_2$ and O linked systems are very sensitive and decompose easily.

Solid state reactivity

The previous sections described the reactivity of Fe(II) precursor complexes with NO$^+$ and NO in solution. Surprisingly, reactivity and a rapid change of color is also observed when exposing solid [Fe(PNP)X$_2$] (X = Cl, Br) to gaseous Nitric Oxide. The reaction of **1a** with NO leads to formation of one major product with v(NO) = 1743 cm^{-1} and a side product with v(NO) = 1867 cm^{-1}. Upon evacuating and heating (ca. 50 °C) of the solid compound for several hours one signal at v(NO) = 1743 cm^{-1} remains. To verify the identity and purity of the obtained product an X-Band EPR Spectrum (Fig. 32) of a solid sample was measured. The splitting of the lines occurs due to hyperfine interaction of the unpaired electron with the iron nucleus (I = 0) and proves the existence of one single low spin species. Using the analogous bromine precursor [Fe(PNP-*i*Pr)FeBr$_2$] (**1a'**) for the same reaction leads to formation of one

major

**Fig. 32 X-Band EPR Spectrum of the vacuum treated reaction product
between [Fe(PNP-*i*Pr)Cl$_2$] and gaseous NO**
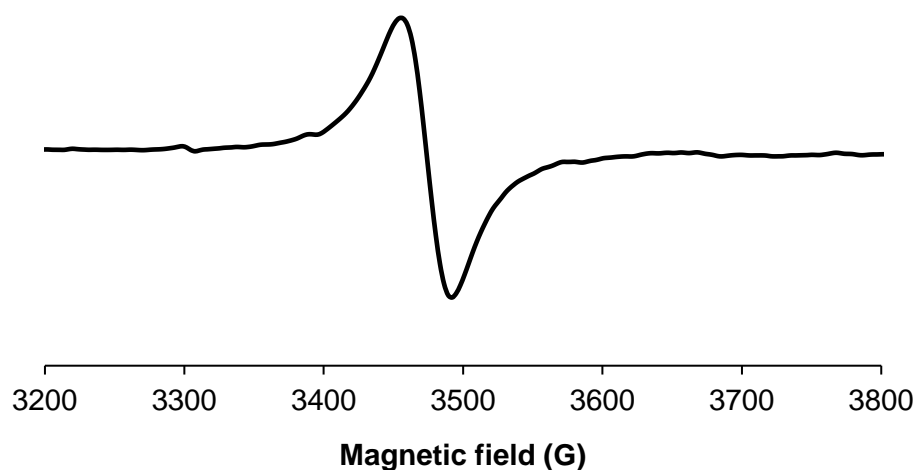
product at v(NO) = 1744 cm^{-1} and two additional components at v(NO) = 1812 cm^{-1} and 1862 cm^{-1}.

This reaction is a formal analogy to the reactivity of **1a** and **1a'** towards CO in solid state[48]. In the case of **1a** one single product, *cis*-[Fe(PNP-*i*Pr)(CO)Cl$_2$] is formed and a mixture of *cis* and *trans* products in the case of the bromine precursor **1a'**. The disappearance of bands after vacuum and heat treatment supports the assumption

that intermediates or instable adducts are formed prior to formation of **2a** or **2a'**. These intermediates can be decomposed thermally to obtain one single low spin iron complex.

3   Conclusion

In the present thesis new attempts to prepare base metal PNP pincer nitrosyl complexes were investigated. Following the preliminary studies by Milstein and Boncella, a series of new low spin Fe(I) complexes of the general composition [Fe(PNP)(NO)X]$^+$ (X = Cl, Br) with PNP being PNP-iPr, PNP^{Me}-iPr and PNP-tBu was prepared by different approaches in solution and in solid state. Both, Nitrosonium salts, which are formally isoelectronic to CO and Nitric oxide react fundamentally different with Fe(II) PNP pincer complexes then does CO. Via a reductive process low valent {FeNO}^{7} compounds with quadratic pyramidal geometry are formed. Surprisingly, these complexes are highly stable for N linked PNP pincer scaffolds but very sensitive for CH$_2$ and O linked PNP systems. The compounds isolated were successfully characterized by means of single crystal X-Ray diffraction, Infrared-, Mössbauer- and EPR-Spectroscopy as well as Mass Spectrometry. Additionally, Density Functional Theory (DFT) was applied to obtain a better understanding of the reaction processes.

4   Experimental part

All manipulations were performed under an inert atmosphere of argon by using Schlenk techniques or in an MBraun inert-gas glovebox. The solvents were purified according to standard procedures. The deuterated solvents were purchased from Aldrich and dried over 4 Å molecular sieves. Nitric oxide (NO 2.5) was purchased from MESSER GmbH (Austria). ^{1}H and ^{31}P{^{1}H} NMR spectra were recorded on a Bruker AVANCE-250 spectrometer. ^{1}H NMR spectra were referenced internally to residual protio-solvent, and solvent resonances, respectively, and are reported relative to tetramethylsilane (d = 0 ppm). ^{31}P{^{1}H} NMR spectra were referenced externally to H_3PO_4 (85%) (d = 0 ppm). Room-temperature solution magnetic moments were determined by ^{1}H NMR spectroscopy using the method of Evans.

CW-EPR spectroscopic analyses were performed on an X-band Bruker Elexsys-II E500 EPR spectrometer (Bruker Biospin GmbH, Rheinstetten, Germany) in solution and in solid state at room temperature. A high sensitivity cavity (SHQE1119) was used for measurements setting the microwave frequency to 9.86 GHz, the modulation frequency to 100 kHz, the center field to 6000 G, the sweep width to 12000 G, the sweep time to 30.0 s, the modulation amplitude to 6 G, the microwave power to 15.9 mW, the conversion time to 7.33 ms and the resolution to 4096 points. The spectra were analyzed using the Bruker Xepr software.

All mass spectrometric measurements were performed on an Bruker Esquire 3000^{plus} 3D-quadrupole ion trap mass spectrometer in positive-ion mode by means of electrospray ionization (ESI). All analytes were dissolved in methanol with hypergrade LC-MS (Merck LiChrosolv) quality.

FT-IR spectra were recorded in solid state on a Bruker Tensor 27 with an ATR unit.

The ^{57}Fe-Mössbauer spectra were recorded with a standard constant-acceleration spectrometer in transmission geometry at 78 K using a continuous flow cryostat. The ^{57}Co source was mounted on the driving system and kept at room temperature. The calibration of the velocity scale was carried out with a α-Fe foil.

Magnetization measurements were performed on powder samples using a Quantum Design MPMS SQUID Magnetometer.

4.1   Synthesis of ligands
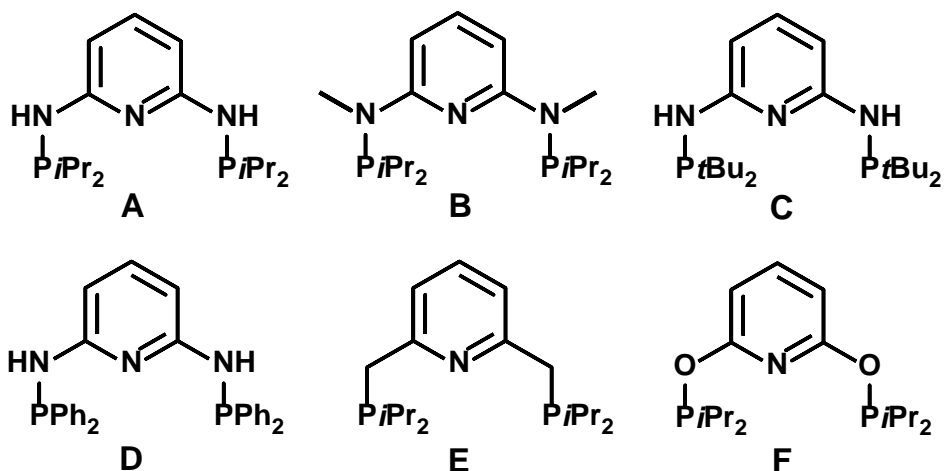
PNP-*i*Pr (A)

To a suspension of 2,6-diaminopyridine (1.00 g, 9.16 mmol) in dry toluene (80 mL) was added Et_3N (3.1 mL, 22.90 mmol). The mixture was cooled to 0 °C and *i*Pr_2PCl (3.1 mL, 19.48 mmol) added drop wise. The reaction mixture was stirred at ambient temperature for 18 h and then filtrated over Celite. The remaining solution was evaporated to dryness and the obtained yellow oil recrystallized from methanol. Yield: 2.44 g (78 %)

^{1}H-NMR (δ, $CDCl_3$): 7.24 (t, 1H, py*H*), 6.44 (dd, 2H, py*H*), 4.30 (d, 2H, N*H*), 1.77 – 1.66 (m, 4H, C*H*(CH_3)_2), 1.10-1.00 (m, 24H, CH(C*H*_3)_2); ^{31}P{^{1}H}-NMR (δ, $CDCl_3$): 47.9

PNP^{CH2}-*i*Pr (E)

To a mixture of 2,6-lutidine (1.5 mL, 12.88 mmol), TMEDA (3.9 mL, 25.76 mmol) and diethyl ether (70 mL) was added a solution of n-BuLi (10.4 mL, 25.92 mmol) at 0 °C with stirring. The orange mixture was stirred at ambient temperature for 4 h and then added slowly *i*Pr_2PCl (4.1 mL, 25.83 mmol) after further cooling to -80 °C. The reaction mixture was stirred at this temperature for 30 min and then at room temperature for further 18 h. The suspension was filtrated of Celite and the remaining solution evaporated to dryness to afford a yellow oil. Yield: 2.62 g (60 %)

^{1}H-NMR (δ, $CDCl_3$): 7.56 (t, 1H, py*H*), 7.23 (d, 2H, py*H*), 3.07 (d, 4H, C*H*_2), 1.96-1.87 (m, 4H, C*H*(CH_3)_2), 1.20-1.15 (m, 24H, CH(C*H*_3)_2); ^{31}P{^{1}H}-NMR (δ, $CDCl_3$): 24.3

PONOP-*i*Pr (F)

To a solution of 2,6-dihydroxypyridine hydrochloride (1.48 g, 10.02 mmol), TMEDA (3 mL, 20.04 mmol) and Triethylamine (8.5 mL, 61.32 mmol) in THF (150 mL) was drop wise added *i*Pr$_2$PCl (3.51 mL, 22.08, mmol) at 0 °C. After the reaction mixture reached room temperature, it was boiled with stirring at 65 °C for 20 h. The obtained suspension was filtrated over Celite and the remaining solution evaporated under vacuum to afford a viscous yellow liquid. Yield: 2.58 g (75 %)

^{1}H-NMR (δ, CDCl$_3$): 7.45 (t, 1H, py*H*), 6.44 (d, 2H, py*H*), 2.08-1.95 (m, 4H, C*H*(CH$_3$)$_2$), 1.25-1.02 (m, 24H, CH(C*H*3)2); ^{31}P{^{1}H}-NMR (δ, CDCl$_3$): 158.0

4.2   Synthesis of complexes

[Fe(PNP-*i*Pr)Cl$_2$] (1a)

PNP-*i*Pr (**A**) (848 mg, 2.48 mmol) and anhydrous FeCl$_2$ (300 mg, 2.36 mmol) were suspended in THF (30 mL) and stirred for 16 h. The solvent was removed in vacuum and the remaining solid washed with pentane (5 mL) twice. The solid was dried in vacuum to obtain a pale yellow product. Yield: 1.05 g (95 %)

[Fe(PNP-*i*Pr)Br$_2$] (1a')

This complex has been prepared analogously to **1a** with **A** (332 mg, 0.97 mmol) and FeBr$_2$ (200 mg, 0.93 mmol) as the starting materials. Yield: 475 mg (92 %)

[Fe(PNP^{Me}-iPr)Cl$_2$] (1b)

PNP^{Me}-*i*Pr (**B**) (459 mg, 1.24 mmol) and anhydrous FeCl$_2$ (150 mg, 1.18 mmol) were suspended in THF (15 mL) and stirred for 16 h. The solvent was removed in vacuum and the remaining solid washed with pentane (5 mL) twice. The solid was dried in vacuum to obtain a yellow product. Yield: 552 mg (94 %)

[Fe(PNP^{Me}-iPr)Br$_2$] (1b')

This complex has been prepared analogously to **1b** with PNP^{Me}-*i*Pr (270 mg, 0.73 mmol) and FeBr$_2$ (150 mg, 0.69 mmol) as the starting materials. Yield: 386 mg (95 %)

[Fe(PNP-*t*Bu)Cl$_2$] (1c)

PNP-*t*Bu (**C**) (329 mg, 0.83 mmol) and anhydrous FeCl$_2$ (100 mg, 0.78 mmol) were suspended in THF (10 mL) and stirred for 20 h. The solvent was removed in vacuum and the remaining solid washed with ether (10 mL) twice. The solid was dried in vacuum to obtain a yellow product. Yield: 364 mg (88 %)

[Fe(PNP-Ph)$_2$Cl]Cl (1d)

PNP-Ph (377 mg, 0.78 mmol) and anhydrous FeCl$_2$ (50 mg, 0.39 mmol) were suspended in THF (10 mL) and stirred for 6 h. The solvent was removed in vacuum and the remaining green solid washed with ether (10 mL) twice. The product was dried in vacuum. Yield: 405 mg (95 %)

[Fe(PNP^{CH2}-*i*Pr)Cl$_2$] (1e)

PNP^{CH2}-*i*Pr (**E**) (281 mg, 0.83 mmol) and anhydrous FeCl$_2$ (100 mg, 0.78 mmol) were suspended in THF (10 mL) and stirred for 20 h. The solvent was removed in vacuum and the remaining solid washed with pentane (10 mL) twice. The solid was dried in vacuum to obtain a yellow product. Yield: 338 mg (92 %)

[Fe(PONOP-*i*Pr)Cl$_2$] (1f)

To a solution of PONOP-*i*Pr (**F**) (284 mg, 0.83 mmol) in THF (10 mL) was added anhydrous FeCl$_2$ (100 mg, 0.78 mmol) and the mixture stirred for 6 h. The solvent was removed in vacuum and the remaining solid washed with pentane (10 mL) twice. The solid was dried in vacuum to obtain a very air sensitive brown-yellow product. Yield: 315 mg (85 %)

[Mn(PNP-*i*Pr)Cl$_2$] (3a)

PNP-*i*Pr (**A**) (228 mg, 0.66 mmol) and anhydrous MnCl$_2$ (80 mg, 0.63 mmol) were suspended in THF (15 mL) and stirred for 16 h. The suspension was reduced to 4 mL and n-pentane (20 mL) was added for precipitation. The off-white powder was collected by filtration and dried under reduced pressure. Yield: 276 mg (93 %)

[Co(PNP-*i*Pr)Cl₂] (4a)

PNP-*i*Pr (**A**) (138 mg, 0.40 mmol) and anhydrous CoCl2 (50 mg, 0.38 mmol) were suspended in THF (15 mL) and stirred for 16 h. The suspension was reduced to dryness and the residual solid washed with pentane (5 mL) twice. The obtained solid was dried in vacuum to give a dark red product. Yield: 165 mg (91 %)

[Fe(PNP-*i*Pr)(NO)Cl]Cl (2a·Cl)

Nitric oxide was bubbled into a solution of **1a** (250 mg, 0.53 mmol) in MeOH (10 mL) for ca. 2 min, whereupon the reaction mixture turned from yellow to purple, and the mixture stirred for 1 h. After the removal of the solvent under reduced pressure, the remaining solid was washed twice with n-pentane (10 mL) and dried under vacuum. Yield: 230 mg (87 %). IR (ATR, cm⁻¹): 1747 (ν_{NO}). μ_{eff} = 1.93 μ_B (EVANS).

[Fe(PNP^{Me}-*i*Pr)(NO)Cl]Cl (2b·Cl)

This complex was prepared analogously to **2a** with **1b** (250 mg, 0.50 mmol) as the starting material. Yield: 236 mg (89 %). IR (ATR, cm⁻¹): 1753 (ν_{NO}).

[Fe(PNP-*t*Bu)(NO)Cl]Cl (2c·Cl)

This complex was prepared analogously to **2a** with **1c** (100 mg, 0.19 mmol) as the starting material. Yield: 88 mg (83 %). IR (ATR, cm⁻¹): 1742.

[Fe(PNP-*i*Pr)(NO)Cl][BF₄] (2a·BF₄)

To a solution of **2a**·Cl (100 mg, 0.20 mmol) in DCM (10 ml) was added AgBF₄ (39 mg, 0.20 mmol) and the mixture stirred for 3 h. The solution was filtrated over Celite, evaporated to dryness and the obtained solid was washed with n-pentane (10 mL). The purple powder was dried under reduced pressure. Yield: 93 mg (85 %). This complex reveals identical IR- and ESI-MS spectra as compared to **2a**·Cl.

General procedure for reactions with nitrosyl salts:

One molar equivalent of [Fe(PNP)X₂] (X = Cl, Br) (**1**) is added to a solution of NOBF₄ or NOSbF₆ in DCM at -30 °C. The reaction mixture is stirred for 1 h, filtrated over Celite and evaporated to dryness. The obtained solid is washed with pentane and dried in vacuum.

General procedure for solid state reactions:

The solid state transformations were carried out using a Schlenk Line connected to a Nitric Oxide bottle. A Schlenk tube with a proper amount of $[(PNP)FeX_2]$ (X = Cl, Br) (**1**) is evacuated an then purged with NO gas. The solid reactant immediately turns brownish purple upon contact with NO and is kept in this atmosphere for 2 h.

5   Appendix

Structural parameters (CCDC) of metal nitrosyl complexes

Bond angle (°)	No.	of	Description
180-170	2058		Linear (l)
170-160	461		Linear (l)
160-150	76		Intermediate (i)
150-140	45		Intermediate (i)
140-130	44		Bent (b)
130-120	54		Bent (b)
120-110	15		Bent (b)
110-100	2		Bent (b)
100-90	1		π-bonded

Extracted from Cambridge Crystallographic Database (www.ccdc.cam.ac.uk)

SQUID measurements of 2a·Cl and 2b·Cl

Inverse of the molar susceptibility for samples: **2a**·Cl (squares) and **2b**·Cl (circles). The lines are the result of linear fits of the modified Curie law to the data. For both samples, an effective moment of 2.2(1) μ_B was obtained from the fit.
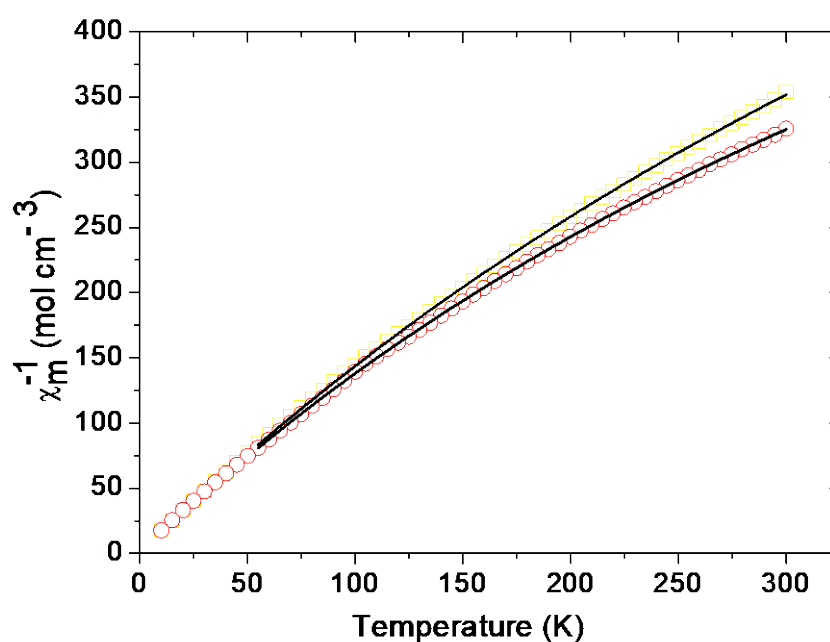
[57]Fe Mössbauer parameters for 2a·Cl and 2b·Cl

The values of the hyperfine parameters obtained from fitting two quadrupole doublets to the experimental spectra are presented in the table below. A residual quantity of a 3rd quadrupole doublet (small impurity or residual reactants) is needed to account for all the experimental peaks of the spectra.

| Sample	Site	IS (mm·s^{-1})	QS (mm·s^{-1})	I (%)
2a·Cl	Blue	0.29(1)	1.28(3)	33.5
	Rose	0.19(1)	1.49(2)	62.9
	Orange	1.21(1)	2.45(2)	3.6
2b·Cl	Blue	0.30(2)	1.27(3)	50.8
	Rose	0.24(3)	1.36(7)	43.5
	Green	0(1)	1.8(4)	5.7

Calculation details

All calculations were performed using density functional theory (DFT) as implemented in the Gaussian 09[49] and ORCA[50] 4.0 software packages on the Vienna Scientific Cluster (VSC3). Geometry optimization were carried out with Gaussian 09 using the TPSS[51] approach to DFT and the 6-311G(d,p) basis set for all atoms. Frequency calculations where performed to confirm the nature of the stationary points yielding no imaginary frequencies. The relative spin-state energies were computed using the TPSS, OPBE, B3LYP and TPSSh exchange-correlation functionals and corrected by adding zero-point vibrational (ZPVE) energies. Further electronic structure calculations, the computation of canonical orbitals, UCOs and QROs were carried out with ORCA. Orbital plots and graphics were generated with Chemcraft[52] 1.8.

Crystal structure determination

X-Ray diffraction data for **2a·**BF$_4$, **2b·**BF$_4$, **2b'·**FeBr$_4$ and **2c·**SbF$_6$ and [Fe(PNP-tBu)(NO)(BF$_4$)][BF$_4$] were collected at T = 100 K in a dry stream of nitrogen on a Bruker KAPPA APEX II diffractometer using graphite-monochromatized Mo Kα radiation (λ = 0.71073 Å) and fine-sliced φ- and ω-scans. Data were reduced to intensity values with SAINT, and an absorption correction was applied with the multiscan approach implemented in SADABS and TWINABS. The structures were solved by methods implemented in SHELXS. The structures were refined using

SHELXL against F^2. Molecular graphics were generated with the program
MERCURY[53].

Crystal Structure of [Fe(PNP^{Me}-*i*Pr)(NO)Br][FeBr$_4$] (2b'·FeBr$_4$)
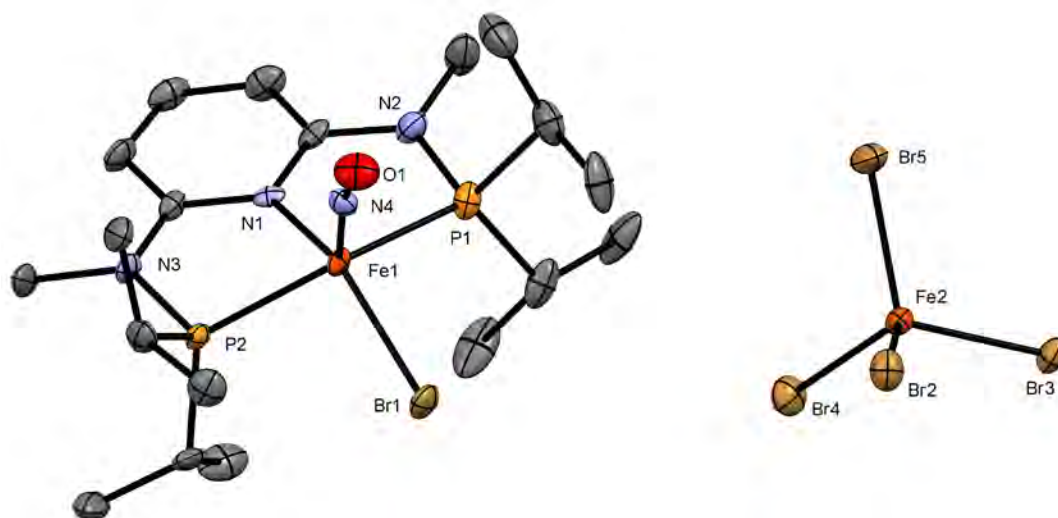
Structural view of [Fe(PNP^{Me}-*i*Pr)(NO)Br][FeBr$_4$] showing 50% displacement ellipsoids (H atoms and solvent molecules omitted for clarity). Selected bond lengths [Å] and angles [°]: Fe1-N1 2.003, Fe1-Br1 2.399, Fe1-P1 2.268, Fe1-P2 2.268, Fe1-N4 1.665, N4-O1 1.184, P1-Fe1-P2 159.21, Fe1-N4-O1 168.50, N1-Fe1-N4 114.72

Crystal Structure of [Fe(PNP-*t*Bu)(NO)(BF$_4$)][BF$_4$]

Due to the highly disordered and badly resolved crystal structure, a Ball and Stick representation is depicted below instead of an ORTEP graph.
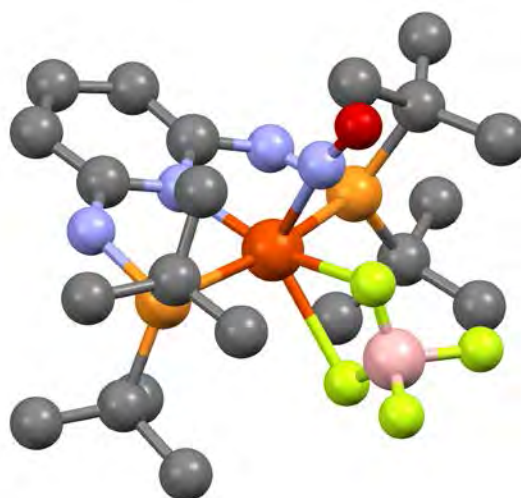
Crystallographic data

	2a·BF$_4$	**2b**·BF$_4$·THF
Empirical formula	C$_{17}$H$_{33}$BClF$_4$FeN$_4$OP$_2$	C$_{23}$H$_{45}$BClF$_4$FeN$_4$O$_2$P$_2$
MW [g/mol]	549.52	649,68
Crystal size [mm]	0.02 x 0.18 x 0.40	0.02 x 0.17 x 0.41
Color, shape	violet, plate	violet, plate
Crystal system	orthorhombic	orthorhombic
Space group	P b c m	P b c n
a [Å]	11.8422(4)	15.3098(7)
b [Å]	9.5011(3)	15.4022(5)
c [Å]	21.9986(6)	23.7855(10)
α [°]	90	90
β [°]	90	90
γ [°]	90	90
V [Å^3]	2475.15(13)	5608.7(4)
Z	4	12
ρ$_{calc}$ [g/cm^3]	1.475	1.453
T [K]	100(2)	100(2)
μ [mm^{-1}]	0.893	0.798
F (0 0 0)	1140	2568
Θ$_{max}$ [°]	27.76	32.65
No. of reflns. measd.	13404	38873
No. of unique reflns.	2993	10071
No. of reflns. I > 2σ	2362	6283
No. of params.	169	340
R$_1$ (all data)	0.0787	0.0990
wR$_2$ (all data)	0.1797	0.1171
GooF	1.145	1.000

Crystallographic data

	2b'·FeBr$_4$	**2c**·SbF$_6$
Empirical formula	C$_{19}$H$_{37}$Br$_5$Fe$_2$N$_4$OP$_2$	C$_{21}$H$_{41}$ClF$_6$FeN$_4$OP$_2$Sb
MW [g/mol]	910.68	754.57
Crystal size [mm]	0.01 x 0.06 x 0.47	0.03 x 0.16 x 0.33
Color, shape	brown, plate	violet, plate
Crystal system	monoclinic	triclinic
Space group	P 21/n	P -1
a [Å]	8.0495(16)	8.1514(16)
b [Å]	30.837(6)	8.2929(17)
c [Å]	12.874(3)	25.045(5)
α [°]	90	88.80(3)
β [°]	97.67(3)	88.93(3)
γ [°]	90	76.73(3)
V [Å^3]	3167.1(11)	1647.3(6)
Z	8	2
ρ$_{calc}$ [g/cm^3]	1.910	1.141
T [K]	100(2)	200(2)
μ [mm^{-1}]	7.345	0.818
F (0 0 0)	1776	568
Θ$_{max}$ [°]	27.83	28.21
No. of reflns. measd.	7087	8600
No. of unique reflns.	7087	8600
No. of reflns. I > 2σ	5254	6893
No. of params.	309	390
R$_1$ (all data)	0.0922	0.1116
wR$_2$ (all data)	0.1135	0.2331
GooF	1.017	1.528

6   Abbreviations

Å	Ångström (0.1 nm)
ATR	Attenuated total reflection
$CDCl_3$	Chloroform, deuterated
Cy	Cyclohexyl
DCM	Dichloromethane, CH_2Cl_2
Et_3N	Triethylamine
DFT	Density Functional Theory
EPR	Electron paramagnetic resonance (- Spectroscopy)
ESI-MS	Electron Spray Ionization Mass Spectrometry
*i*Pr	iso-propyl
iPr_2PCl	Chlorodiisopropylphosphine
IR	Infrared (- Spectroscopy)
Me	Methyl (i.e. CH_3)
MeOH	Methanol
NMR	Nuclear Magnetic Resonance (- Spectroscopy)
NO	Nitric Oxide
ORTEP	Oak Ridge Thermal Ellipsoid Plot
Ph	Phenyl
*t*Bu	tert.-Butyl
THF	Tetrahydrofurane
TMEDA	Tetramethylethylenediamine
XRD	X-Ray Diffraction

7   Bibliography

(1)   Bauer, G.; Hu, X. *Inorg. Chem. Front.* **2016**, *3*, 741–765.

(2)   Garbe, M.; Junge, K.; Beller, M. *European J. Org. Chem.* **2017**, *2017* (30), 4344–4362.

(3)   Van Koten, G. *J. Organomet. Chem.* **2013**, *730*, 156–164.

(4)   Morales-Morales, D. *Rev. la Soc. Química México* **2004**, *48* (Ii), 338–346.

(5)   Moulton, B. C. J.; Shaw, B. L. *Dalt. Trans.* **1975**, No. 1020, 1020–1024.

(6)   Benito-Garagorri, D.; Becker, E.; Wiedermann, J.; Lackner, W.; Pollak, M.; Mereiter, K.; Kisala, J.; Kirchner, K. *Organometallics* **2006**, *25* (8), 1900–1913.

(7)   Salem, H.; Shimon, L. J. W.; Diskin-Posner, Y.; Leitus, G.; Ben-David, Y.; Milstein, D. *Organometallics* **2009**, *28* (16), 4791–4806.

(8)   Jansen, A.; Pitter, S. *Monatshefte für Chemie / Chem. Mon.* **1999**, *130* (6), 783–794.

(9)   Tolman, C. A. *Chem. Rev.* **1977**, *77* (3), 313–348.

(10)   Janzen, D. E.; Hang, M.; Kaup, H. M. In *ACS Symposium Series*; 2013; Vol. 1128, pp 155–168.

(11)   Karen, P. *Angewandte Chemie - International Edition.* 2015, pp 4716–4726.

(12)   Kaim, W.; Schwederski, B. *Coord. Chem. Rev.* **2010**, *254* (13–14), 1580–1588.

(13)   McCleverty, J. A. *Chem. Rev.* **2004**, *104* (2), 403–418.

(14)   Mingos, D. M. P. *Nitrosyl Complexes in Inorganic Chemistry , Biochemistry and Medicine I*; 2014.

(15)   Ford, P. C.; Lorkovic, I. M. *Chem. Rev.* **2002**, *102* (4), 993–1017.

(16)   Enemark, J. H.; Feltham, R. D. *Coord. Chem. Rev.* **1974**, *13* (4), 339–406.

(17)   Navaza, A.; Chevrier, G.; Alzari, P. M.; Aymonino, P. J. *Acta Crystallogr. Sect. C Cryst. Struct. Commun.* **1989**, *45* (6), 839–841.

(18)   Butler, A. R. *J. Chem. Educ.* **1982**, *59* (7), 549.

(19)   Marchlewksi, L.; Sachs, J. *Zeitschrift fur Anorg. und Allg. Chemie* **1860**, *2*, 175–181.

(20)   Lin, Z. S.; Chiou, T. W.; Liu, K. Y.; Hsieh, C. C.; Yu, J. S. K.; Liaw, W. F. *Inorg. Chem.* **2012**, *51* (19), 10092–10094.

(21)   Hieber, W.; Beutner, H. *Zeitschrift fur Anorg. und Allg. Chemie* **1963**, *320* (1–4), 101–111.

(22)   Connelly, N. G.; Gardner, C. *J. Chem. Soc. Dalt. Trans.* **1976**, *1976* (16),

1525–1527.

(23)   Hames, B. W.; Legzdins, P.; Martin, D. T. *Inorg. Chem.* **1978**, *17* (12), 3644–3647.

(24)   Hayton, T. W.; Legzdins, P.; Sharp, W. B. *Chem. Rev.* **2002**, *102*, 935–991.

(25)   Caulton, K. G. *Coord. Chem. Rev.* **1975**, *14*, 317–355.

(26)   Richter-Addo, G. B.; Legzdins, P.; Burstyn, J. *Chem. Rev.* **2002**, *102* (4), 857–859.

(27)   Mingos, D. M. P.; Sherman, D. J. *Adv. Inorg. Chem.* **1989**, *34*, 293–377.

(28)   Feller, M.; Ben-Ari, E.; Gupta, T.; Shimon, L. J. W.; Leitus, G.; Diskin-Posner, Y.; Weiner, L.; Milstein, D. *Inorg. Chem.* **2007**, *46* (25), 10479–10490.

(29)   Gaviglio, C.; Ben-David, Y.; Shimon, L. J. W.; Doctorovich, F.; Milstein, D. *Organometallics* **2009**, *28* (6), 1917–1926.

(30)   Fogler, E.; Iron, M. A.; Zhang, J.; Ben-David, Y.; Diskin-Posner, Y.; Leitus, G.; Shimon, L. J. W.; Milstein, D. *Inorg. Chem.* **2013**, *52* (19), 11469–11479.

(31)   Choualeb, A.; Maccaroni, E.; Blacque, O.; Schmalle, H. W.; Berke, H. *Organometallics* **2008**, *27* (14), 3474–3481.

(32)   Tondreau, A. M.; Boncella, J. M. *Polyhedron* **2016**, *116*, 96–104.

(33)   Trovitch, R. J.; Lobkovsky, E.; Chirik, P. J. *Inorg. Chem.* **2006**, *45* (18), 7252–7260.

(34)   Pelczar, E. M.; Emge, T. J.; Krogh-Jespersen, K.; Goldman, A. S. *Organometallics* **2008**, *27* (22), 5759–5767.

(35)   Ingleson, M. J.; Fullmer, B. C.; Buschhorn, D. T.; Fan, H.; Pink, M.; Huffman, J. C.; Caulton, K. G. *Inorg. Chem.* **2008**, *47* (2), 407–409.

(36)   Ehrlich, N.; Kreye, M.; Baabe, D.; Schweyen, P.; Freytag, M.; Jones, P. G.; Walter, M. D. *Inorg. Chem.* **2017**, *56* (14), 8415–8422.

(37)   Lyaskovskyy, V.; De Bruin, B. *ACS Catalysis.* 2012, pp 270–279.

(38)   Dudle, B.; Rajesh, K.; Blacque, O.; Berke, H. *J. Am. Chem. Soc.* **2011**, *133* (21), 8168–8178.

(39)   Jiang, Y.; Blacque, O.; Fox, T.; Freeh, C. M.; Berke, H. *Chem. - A Eur. J.* **2009**, *15* (9), 2121–2128.

(40)   Plietker, B. *Angew. Chemie - Int. Ed.* **2006**, *45* (9), 1469–1473.

(41)   Cramer, C. J.; Truhlar, D. G. *Phys. Chem. Chem. Phys.* **2009**, *11* (46), 10757–10816.

(42)   Tomson, N. C.; Crimmin, M. R.; Petrenko, T.; Rosebrugh, L. E.; Sproules, S.; Christopher Boyd, W.; Bergman, R. G.; Debeer, S.; Dean Toste, F.; Wieghardt, K. *J. Am. Chem. Soc.* **2011**, *133* (46), 18785–18801.

(43) Kupper, C.; Schober, A.; Demeshko, S.; Bergner, M.; Meyer, F. *Inorg. Chem.* **2015**, *54* (7), 3096–3098.

(44) Boguslawski, K.; Jacob, C. R.; Reiher, M. *J. Chem. Theory Comput.* **2011**, *7* (9), 2740–2752.

(45) Neese, F. *J. Phys. Chem. Solids* **2004**, *65* (4), 781–785.

(46) Benito-Garagorri, D.; Alves, L. G.; Puchberger, M.; Mereiter, K.; Veiros, L. F.; Calhorda, M. J.; Carvalho, M. D.; Ferreira, L. P.; Godinho, M.; Kirchner, K. *Organometallics* **2009**, *28* (24), 6902–6914.

(47) Bichler, B.; Glatz, M.; Stöger, B.; Mereiter, K.; Veiros, L. F.; Kirchner, K. A. *Dalt. Trans.* **2014**, *43* (39), 14517–14519.

(48) Benito-Garagorri, D.; Puchberger, M.; Mereiter, K.; Kirchner, K. *Angew. Chemie - Int. Ed.* **2008**, *47* (47), 9142–9145.

(49) Frisch, M. J.; Trucks, G.W.; Schlegel, H. B.; Scuseria, G. E.; Robb, M. A.; Cheeseman, J. R.; Scalmani, G.; Barone, V.;Mennucci, B.; Petersson, G. A.; Nakatsuji, H.; Caricato, M.; Li, X.; Hratchian, H. P.; Izmaylov, A. F.; Bloino, J.; Zheng, G.; Sonnenber, D. J. *Gaussian, Inc. Wallingford CT* **2009**, 2–3.

(50) Neese, F. *Wiley Interdiscip. Rev. Comput. Mol. Sci.* **2012**, *2* (1), 73–78.

(51) Perdew, J. P.; Ruzsinszky, A.; Tao, J.; Staroverov, V. N.; Scuseria, G. E.; Csonka, G. I. *J. Chem. Phys.* **2005**, *123* (6).

(52) www.chemcraftprog.com/. .

(53) Macrae, C. F.; Edgington, P. R.; McCabe, P.; Pidcock, E.; Shields, G. P.; Taylor, R.; Towler, M.; Van De Streek, J. *Journal of Applied Crystallography*. 2006, pp 453–457.